# Mechanisms and Free Energies of Enzymatic Reactions

**Jiali Gao**[*], **Shuhua Ma**, **Dan T. Major**, **Kwangho Nam**, **Jingzhi Pu**, and **Donald G. Truhlar**[*]
Department of Chemistry and Supercomputing Institute, Digital Technology Center, University of Minnesota, Minneapolis, Minnesota 55455

## 1. Introduction

Most enzymatic reactions have very large and remarkably similar apparent second-order rate constants, $k_{cat}/K_M$, at mean values of about $10^7$ M$^{-1}$ s$^{-1}$ with $k_{cat}$ in the range of 10–1000 s$^{-1}$.[1–3] In fact, many reactions approach the diffusional encounter rate at the limited enzyme concentration ($<10^{-5}$ M) in the cell.[4] Wolfenden illustrated the catalytic power of enzymes by comparing the rate constant of the catalyzed reaction with that of the same reaction in the absence of the enzyme in aqueous solution, $k_{aq}$.[2,5] Evidently, the most proficient enzymes are those catalyzing the slowest spontaneous reactions, such as the hydrolysis of glycosides and phosphate esters and the decarboxylation reactions of amino acids and of orotidine 5′-monophosphate (OMP), as catalyzed by OMP decarboxylase (ODC).[2] In the latter case, the unimolecular rate constant of the spontaneous decarboxylation of OMP is accelerated ($k_{cat}/k_{aq}$) by 17 orders of magnitude in the active site of ODC.[5,6] This reaction also has the distinction of being among the most proficient enzymes in catalyzing reactions without the involvement of cofactors. Significantly, Wolfenden's experimental approach has been followed and paralleled in computational studies.[7] The experiments, along with computational results that we review in this article, provide abundant evidence that the very large observed reductions of the free energy of activation can be achieved through the strong synergism of enzyme and substrate interactions "using ordinary noncovalent forces of attraction",[8] although in other cases enzyme catalysis may involve covalent intermediates[9] or a change in reaction mechanism as compared to aqueous solution.

Noncovalent attractive forces are mainly electrostatic in nature; they include ion pair interactions, hydrogen bonding, and electronic polarization. The competition between solvent–solvent and solvent–solute interactions contributes to hydrophobic effects (where the "solute" is the substrate or any part of the protein or a coenzyme that participates in the reaction coordinate and the "solvent" is water, spectator residues of the enzyme in the active site, and faraway parts of the protein or protein complex). These interactions all contribute to catalysis. It has been argued insightfully that electrostatic preorganization effects are a key source of enzyme catalysis,[10] but the questions remain of what other factors contribute and how preorganization is arranged such that the transition state is stabilized preferentially to the reactant state. To understand enzyme catalysis and mechanism, it is necessary, and

[*]gao@chem.umn.edu; truhlar@umn.edu.

often challenging, to elucidate the unique ways in which each enzyme exerts electrostatic and other forces on the substrate and the transition state.

In the past 10 years, many computational studies of enzymatic reactions have been carried out, combining quantum mechanical, classical mechanical, and statistical mechanical techniques, coupled with advances in protein structure determination, site-directed mutagenesis, and fast computers and algorithms. All computational studies of atomic scale dynamics must begin with a potential energy surface, and the most promising approach to calculating this surface is to treat the enzyme active site by electronic structure methods[11–19] that include the electronic polarization of the reactive species by the dynamical fluctuations of the enzyme–solvent environment through effective sampling of the enzyme conformational space. Although a review necessarily involves only a very limited selection of the reactions that enzymes catalyze in the cell, we can nevertheless conclude[7] that each enzyme has its unique characteristics, and enzymes use all possible means to achieve the ultimate objective of reducing the free energy of activation.

In addition to providing an enormous rate acceleration, enzymes exercise precise control over the regio- and stereochemistry of the reactions that they catalyze, an aspect of enzyme catalysis that has received relatively little attention in computations (recent studies of triosephosphate isomerase and glyoxal synthase provide a noteworthy exception[20]). This control is perhaps best illustrated by the reactions catalyzed by terpenoid synthases,[21] a large group of enzymes that transform a limited number of linear substrates such as geranyl diphosphate (C10), farnesyl diphosphate (C15), and geranylgeranyl diphosphate (C20) to tens of thousands natural products with a variety of rings and stereocenters, presumably by prefolding the same substrate to a "proper" conformation in the unique binding pocket of each enzyme and subsequently preventing the highly reactive carbocation intermediates from undergoing side reactions and preventing premature terminations of the catalyzed reaction sequences. Both experimental and computational studies appear to point to an important role for the balance of thermodynamic and kinetic factors along the cyclization cascade.[22,23] Thus, it is of great interest not only to understand the origin of the enormous catalytic power of enzymes that they achieve by lowering the free energy of activation but also to characterize the detailed mechanism of enzyme actions that control each reaction step and provide the desired regio- and stereospecificity.

In this review, we summarize computational studies of the mechanisms and free energies of selected enzymatic reactions. We first highlight computational approaches for enzymatic reactions, with special emphasis on two key elements that affect the computational accuracy, namely, the potential energy function and statistical mechanical sampling of the enzyme system. The potential energy functions may be based on quantum mechanical models, or they may be based on molecular mechanics force fields. In either case, to achieve the required accuracy to understand catalysis, it is essential to parametrize and validate the potential energy functions (or, equivalently, the methods used to calculate them) against model reactions and specific hydrogen bonding interactions in the gas phase. Only when the performance of the potential functions on the intrinsic reactivity of the chemical reactions has been justified can one begin to address the key questions of solvent effects and enzyme catalysis through molecular dynamics and free energy simulations. We then discuss a third

element, namely, the choice of the reaction coordinate for determining the free energy of activation to characterize the mechanism of enzymatic processes. Then, we illustrate a variety of factors that have been found to contribute to catalysis in specific enzymatic reactions by lowering the free energy of activation relative to that for the uncatalyzed process in aqueous solution. Finally, we provide a summary of the major conclusions.

## 2. Methods for Computational Studies of Enzymatic Reactions in Aqueous Solution

In this section, we present a brief summary of the theory and key computational techniques that we use for studying chemical reactions catalyzed by enzymes and the corresponding uncatalyzed reactions, both in aqueous solution.

### 2.1. Generalized Transition State Theory

Generalized transition state theory (TST) provides a theoretical framework for understanding chemical reactions in the gas phase, in solution, and in enzymes. Conventional[24,25] and generalized[26] transition state theory were originally developed for gas-phase reactions, but transition state theory is readily generalized to liquid-phase reactions,[27] and it has become the framework for both qualitative and quantitative studies of reactions catalyzed by enzymes. The rate constant for a reaction at temperature $T$ can be conveniently expressed as follows:

$$k(T) = \gamma(T) k^{\mathrm{TST}}(T) = \gamma(T) \frac{1}{\beta h} e^{-\beta \Delta G^{\ddagger}(T)} \quad (1)$$

where $\beta = 1/(k_{\mathrm{B}} T)$, $k_{\mathrm{B}}$ being Boltzmann's constant, $h$ is Planck's constant, and $k^{\mathrm{TST}}$ is the transition state theory rate constant. The transmission coefficient, $\gamma(T)$, which has a value of unity in simple transition state theory, has three components,[7]

$$\gamma(T) = \Gamma(T) \kappa(T) g(T) \quad (2)$$

which account for, respectively, dynamical recrossing of the transition state hypersurface that separates the reactants and products, quantum mechanical tunneling in the reaction coordinate, and nonequilibrium distributions in phase space. Note that $\gamma(T)$, $\kappa(T)$, and $\Gamma(T)$ are called, respectively, the transmission coefficient, the tunneling transmission coefficient, and the recrossing transmission coefficient.

In eq 1, $G^{\ddagger}(T)$ is the molar standard-state quasithermodynamic free energy of activation, which is related to the potential of mean force, $W(T,q)$, also called the PMF, by eq 3,[28,29]

$$\Delta G^{\ddagger}(T) = W(T, q^{\ddagger}) - [W(T, q_{\mathrm{R}}) + G^{\mathrm{R}}(q)] + C(T, q) \quad (3)$$

where $q^{\ddagger}$ and $q_{\mathrm{R}}$ are values of the reaction coordinate, $q$, at the transition state and reactant state, respectively, $G^{\mathrm{R}}(q)$ corresponds to the free energy of the mode in the reactant state, R, which correlates with the reaction coordinate, and $C(T,q)$ is a correction term that is due to the Jacobian of the transformation from a locally rectilinear reaction coordinate to the

curvilinear reaction coordinate, $q$.[29] This correction term is often small and is usually neglected. The potential of mean force is defined by[30]

$$W(T,q) = -RT\ln\rho(T,q) + W^0 \quad (4)$$

where $\rho(T,q)$ is the classical mechanical probability density as a function of the reaction coordinate, and $W^0$ is a constant of integration that may be regarded as setting the zero of free energy.

Equation 1 shows that there are two contributing quantities to be evaluated to determine the rate constant for the reaction: the quasithermodynamic free energy of activation, $G^{\ddagger}(T)$, and the transmission coefficient, $\gamma(T)$. However, this separation of $G^{\ddagger}(T)$ and $\gamma(T)$ is not unique because both the calculation of the potential of mean force and the determination of the transmission coefficient depend on the definition of the reaction coordinate. These quantities also both depend on the dynamic fluctuations of the protein and solvent,[31] and thus various physical effects may show up in one or another of these, depending on the extent to which the protein and the solvent are included in the definition of the reaction coordinate. Computational studies show that the dominant factor responsible for the rate enhancement by enzymes is the lowering of the free energy of activation as compared to that of the uncatalyzed reaction in water.[7,32,33] Nevertheless the transmission coefficient is also critical for understanding enzyme dynamics. It is sensitive to substrate–enzyme, substrate–cofactor, and substrate–water interactions, and it can either accelerate or decelerate reactions, depending on whether a given change in the system or surroundings increases or decreases $\gamma(T)$. However, the transmission coefficient contributes no more than a factor of $\sim 10^3$ to the reaction rate. Although $10^3$ is a large number, this effect is small when compared to the maximum effect achieved by lowering the equilibrium free energy of activation; the latter effect has been found to accelerate the reaction rate by as much as a factor of $10^{19}$. Thus, most of the effort in computational enzymology, which is the main subject of this paper, has been the development and applications of computational methods that can yield accurate results for $G^{\ddagger}(T)$ both for the enzymatic reaction and for the uncatalyzed solution reaction. An accompanying article in this issue describes in more detail the dynamical and quantum mechanical factors,[34] especially tunneling and recrossing, that contribute to the transmission coefficient for enzyme-catalyzed reactions.

The catalytic effect, or rate enhancement, of an enzyme on a unimolecular reaction can be defined as the ratio of the rate constant for the enzymatic reaction to that for the uncatalyzed process in aqueous solution, $k_{cat}/k_{aq}$, or equivalently, the difference in quasi-thermodynamic free energy of activation between the catalyzed and uncatalyzed reactions, assuming that the transmission coefficients cancel out:

$$\Delta\Delta G^{\ddagger}(T) = \Delta G^{\ddagger}_{cat} - \Delta G^{\ddagger}_{aq} \quad (5)$$

where $\Delta G^{\ddagger}_{cat}$ and $\Delta G^{\ddagger}_{aq}$ are, respectively, the quasi-thermodynamic free energy of activation for the enzymatic and the uncatalyzed reaction. This definition is fully justified when substrate concentration is high such that the enzyme is saturated, and the reaction is unimolecular with rate constant $k_{cat}$. It is still important and of particular interest when the

substrate concentration is low, in which case the ratio $k_{cat}/K_M$ is the *apparent* second-order rate constant,[35] because it provides an understanding of the key chemical question of how the rate of the chemical transformation is accelerated by the enzyme. Here, $K_M$ is the Michaelis constant. This comparison, however, can be complicated by the involvement of cofactors and oxidation–reduction reactions at metal centers as well as by a possible change in reaction mechanism from aqueous solution to the enzyme active site, although these factors can easily be incorporated into this framework.

The pseudothermodynamic cycle of Scheme 1 has often been used to stress Pauling's concept of an enzyme's high affinity for the transition state over that for the substrate,[2,36,37] in which the apparent equilibrium constant $K_{TS} = (k_{cat}/K_M)/k_{aq}$ provides a measure of the proficiency of enzyme catalysis.[2] However, this equilibrium is never directly measured nor even achieved in part because the transition state of the enzymatic reaction may be very different from that of the uncatalyzed reaction and in part because the E•S$^{\ddagger}$ state developed during the enzymatic process may be entirely different from that of a physical binding process of S$^{\ddagger}$ by E.[38] Many examples show that the X-ray crystal structures of enzyme–substrate analogues and enzyme–transition state inhibitors can be very different from the real substrate–enzyme structures.[39–42] In fact, it is possible to over-interpret the pseudothermodynamic cycle of Scheme 1 in computational studies.[43,44] Although $k_{cat}$ and $k_{aq}$ can be determined reasonably accurately (at least for a given potential energy surface) and their ratio even more accurately by molecular dynamics simulations using umbrella sampling (see below), it is more difficult to obtain accurate results for $K_M$ and $K_{TS}$ when free energy perturbation (FEP) techniques are used because these calculations necessarily involve the annihilation of the substrate and the distorted substrate in the transition state in the active site.[45] If the enzyme samples very different conformational substates when S and S$^{\ddagger}$ are present, the computed results will not lead to a closed form as shown in Scheme 1, that is, $k_{cat}/k_{aq}$ $K_{TS}K_M$.[43,44] Thus, the attempt to equate $k_{cat}k_{aq}$ to $K_{TS}K_M$ as a proof or justification of computational consistency is not guaranteed.[46,47] On the contrary, analyses of the inequality of these two ratios, determined separately using different computational approaches (see below), can provide valuable information on specific contributions to catalysis due to the changes in enzyme conformation along the reaction pathway.

## 2.2. Potential Energy Functions

The potential energy function describes the energetic changes involved in rearranging the substrate, including the changes in substrate–enzyme, substrate–cofactor, and substrate–water interactions. The accuracy of the potential energy function used to carry out molecular dynamics simulations has a large effect on the reliability of the computed $G^{\ddagger}(T)$ and, consequently, on the conclusions about the origin of enzyme catalysis.[12,13] Achieving high accuracy in the potential energy function is difficult because it is necessary to obtain the potential energy function by a method capable of modeling the formation and breaking of chemical bonds. The construction of potential energy functions for molecular dynamics calculations of enzymatic reactions needs to balance computational efficiency and accuracy.[48] In this review, we only consider thermal enzyme reactions (i.e., not photochemical reactions), and we only consider the lowest Born–Oppenheimer electronically adiabatic potential energy surface,[49] which is sufficient for most purposes. We

classify the potential energy functions that have been used into three types, which are briefly discussed below.

**2.2.1. Potentials from Empirical Force Fields—**The first is the use of analytical functions fitted to reproduce key energetic and structural results either from experiments or from high-level ab initio calculations. This approach, when the analytic function is expressed in terms of transferable parameters for valence interactions (stretches, bends, and torsions), van der Waals nonbonded interactions, and electrostatics, is called molecular mechanics (MM) or force fields. It has been widely used in many areas. Some specific MM force fields mentioned below are CHARMM22[50] and GROMOS.[51] Recent reviews of MM methods have been provided by MacKerell,[52] Cramer,[53] and Ponder and Case.[54]

The application of MM methods to modeling solute–solvent interactions in uncatalyzed chemical reactions in solution was pioneered by Chandrasekhar and Jorgensen in their classic study of a model $S_N2$ reaction in water.[55,56] Their study involved three key steps: (1) defining a reaction path, (2) determining potentials that reproduce experimental or ab initio results for both structures and energies along the entire reaction path in the gas phase and that adequately describe solute–solvent interactions, and (3) performing free energy simulations. This procedure remains valuable for studying chemical reactions in solution and in enzymes. Variants of this procedure include the quantum-mechanics-plus-free-energy (QM+FE) approach proposed by Kollman and coworkers,[57] in which a reaction path is determined in the gas phase or in a given enzyme environment, followed by free energy (FE) simulations using a potential that is fitted to reproduce the polarized charge distribution of the reacting species along this fixed path. Yang and co-workers further developed and applied this approach in a number of calculations of enzymatic reactions, using the reaction path and charges derived from combined QM/MM energy minimizations (the QM/MM method is explained as type 3 below) and density functional theory (DFT).[58,59]

Another type-1 approach for deriving potential functions, which has been extensively used in modeling chemical reactions in solution and in enzymes, is the empirical valence bond (EVB) method.[60] The key feature of the EVB method is the construction of the potential energy function by a combination of molecular mechanics force fields for the reactant and product electronically diabatic states, and this combination follows a procedure akin to quantum mechanical valence bond theory. (There are many empirical approaches based on valence bond theory, but we use the acronym EVB for a particular one of them, pioneered by Warshel and Weiss,[61] and others are called semiempircial valence bond theory in general or by special names such as London–Eyring–Polanyi–Sato theory,[62–64] diatomics-in-molecules theory,[65] multiconfiguration molecular mechanics,[66] and so forth.) Although, in principle, many valence bond states can be included in constructing an EVB potential, and sometimes this is done, most applications to enzymatic reactions have employed a simple two-state procedure.[47,67] The reactant and product states are considered to be effective valence bond states that incorporate nonunique combinations of many Lewis resonance structures, and consequently, the charge distributions of the effective valence bond states are geometry-dependent.[68–70] The EVB method has been used widely.[10,32,33,46,67,71–73] The success in many applications seems to originate from the parametrization of the resonance integral $\varepsilon_{12}$ to the barrier height of the specific reaction and of the diagonal constant $\varepsilon$ to

the free energy of reaction.[60,67] The parametrization process or calibration has been typically carried out for the uncatalyzed reaction in aqueous solution,[10,32] and then, the study of enzymatic reactions is performed to estimate $G^{\ddagger}(T)$ using these parameters. Although this is reasonable for studying catalytic effects in terms of $G^{\ddagger}(T)$, solvent effects are not directly computed, but rather they are fitted by adjusting the two empirical matrix elements. It should be noted that the lack of charge variation (mentioned above) as a function of the reaction coordinate for each effective valence bond state can cause the method to overestimate the solvent reorganization energy.[70] In principle, this lack of charge variation is not a limitation, because it can be overcome by fitting against electronic structure calculations or by following a parametrization procedure like Jorgensen's. One difficulty with EVB calculations in the literature is that often the values of the parameters or even the precise functional form used for the critical resonance integral is not given. Furthermore, it seems that the resonance integral is sometimes replaced by a geometry-independent constant, whereas careful checks of this approximation for gas-phase reactions show that it can yield nonphysical results, at least for some choices of MM parameters.[66] Here, we note that the central guideline[74] for publication of computational results is that the author should provide enough details that a calculation could in principle be reproduced.

**2.2.2. Ab Initio and DFT Potentials**—The second type of potential function for studying chemical reactions is based on first-principles models, with the entire enzyme–solvent system treated by quantum mechanics.[75–83] Although this approach has the advantage of avoiding the intermediate parametrization step and has been applied successfully to a variety of condensed-phase systems, including torsional potentials in enzymes,[83] the computational costs are still too large to be practical for free energy simulations of enzymatic reactions with appreciable barriers.

One can also treat the entire system by quantum mechanics but use a semiempirical molecular orbital approach rather than first-principles quantum mechanics.[84–87] This approach is intermediate between type 2 above and type 3 below.

**2.2.3. Combined QM/MM Potentials**—The third type of potential energy function, which currently provides the most practical and reliable approach for free energy simulations, is the combination of quantum mechanics and molecular mechanics; potentials obtained this way are called combined QM/MM potentials.[12,13,80,88–92] This method was first described in the pioneering work of Warshel and Levitt in 1976,[88] although its potential was not fully appreciated until the 1990s. In this approach, the substrate and amino acids directly participating in bond formation (and maybe all or part of the cofactor) are treated by quantum mechanical electronic structure theory, and the remainder of the protein and aqueous solvent is represented by force fields. The method combines the applicability of quantum mechanical methods to bond rearrangement processes with the computational efficiency of molecular mechanics for large molecular systems, and the quantum mechanical part can in principle be made accurate and reliable. The use of an explicit electronic structure method to describe the enzyme active site is important because understanding the changes in electronic structure along the reaction path can help to design inhibitors and novel catalysts. It is also important because the dynamic fluctuations of the enzyme and

aqueous solvent system have a major impact on the polarization of the species involved in the chemical reaction, which, in turn, affects the chemical reactivity.[93,94] Analytical potentials typically do not include electronic polarization effects explicitly, and thus such methods might not properly reflect the change in the potential surface as the protein undergoes dynamical fluctuations (due both to Coulombic and internal bonding terms). Combined QM/MM potentials and their applications have been reviewed in a number of publications.[11,13,76,90,92,95–98]

The most popular methods for treating the quantum mechanical subsystem in QM/MM studies of enzymatic reactions have been molecular orbital methods such as the semiempirical MNDO (modified neglect of differential overlap),[99] AM1 (Austin model 1),[100] and PM3 (parametrized model 3) models,[101] ab initio Hartree–Fock (HF) theory and Møller–Plesset perturbation theory (MP2),[102] and density functional theory (DFT).[103] In DFT calculations, the hybrid three-parameter B3LYP functional[104] has often been used, whereas the Becke–Lee–Yang–Parr functional[105,106] is typically adopted in many Car–Parrinello molecular dynamics simulations.[77–80] In most cases, the mPW1PW91 functional,[107] which has a similar form to the B3LYP one, is more accurate, but it has been less widely used. Several relatively new functionals[108,109] including a dependence on kinetic energy density and having improved performance for barrier heights and noncovalent interactions have not yet seen use for enzyme simulations. Although first principles methods such as DFT are very appealing even when combined with MM,[289–292] they are still too slow to allow sufficient sampling of the enormous number of enzyme conformational states to obtain the potential of mean force along the reaction coordinate. In fact, the ability to sample enzyme conformational space is the second most important issue in computational studies of enzymatic reactions. For example, early simulations in which the protein system was allowed to relax demonstrated the importance of such relaxation for determining side chain torsional potentials and the effects of ligand binding in myoglobin.[110,111] The work of Bruice and coworkers showed the insight that can be obtained by analyzing the conformational substates that are most favorable for transition state stabilization.[36,112,113] Those reactant-like substates are often in the region of configuration space where molecular mechanics may be used, but a fuller analysis of reactivity requires knowing the potential where molecular mechanics is not valid. Thus, in deciding which potential energy function shall be used in studying enzymatic reactions, one must consider its capability to effectively sample protein conformational space along the entire reaction pathway.

An appealing feature of ab initio and DFT methods is that the accuracy can often be improved by using larger basis sets and, in wave function theory, by better describing the electron correlation (in DFT, there are no systematic methods for improving the description of correlation.). Currently, though, semiempirical QM/MM models are the only practical approach allowing reasonable sampling of enzyme conformations in molecular dynamics simulations, although first-principles-based DFT methods are emerging for use as the QM part of QM/MM potentials in short molecular dynamics calculations. The limitation of semiempirical QM methods is that they are not very accurate for most reactions to be studied, and it is necessary to improve and validate the performance of the semiempirical Hamiltonian for each specific application. One approach is to develop specific reaction parameters (SRP) for the reaction of interest by reproducing the structures and energies from

experiments and reliable calculations.[114–119] Because the shape of the potential energy surface is usually well represented by semiempirical models, an even simpler approach is to add a semiempirical valence bond term such as the London–Eyring–Polanyi–Sato function or even a simple valence bond function to correct the errors in the computed energy of activation and energy of reaction.[120–122] Although it differs in functional form, this strategy has some similarity to the recent development of the PDDG models that reparametrize the empirical Gaussian terms for core–core interactions.[123,124] These improved model Hamiltonians can provide results as accurate as the target data for the model systems, and they have been used in the study of several enzymatic reactions.[125,126]

Semiempirical QM/MM methods can be combined with high-level ab initio results, typically from MP2 or DFT calculations, by using a dual-level approach.[127–130] Here, the QM/MM energy is separated into a solvent/enzyme-independent term, which is the energy of the QM model in the gas phase, and a substrate–enzyme interaction component. In general, the errors in semiempirical QM models originate from its intrinsic performance for the reaction in the gas phase, that is, the first term of this separation, and we use the results from a high-level (HL) method to replace it. QM/MM interaction energies can be obtained accurately even when a lower-level (LL), semiempirical QM/MM Hamiltonian is used because one can always parametrize the non-bonded van der Waals terms, and these terms are always present and need to be parametrized for each QM model, whether it is a semiempirical or an ab initio/DFT method.[131–133] In short, in dual-level QM/MM calculations, the enzyme conformational sampling is carried out using the computationally efficient, semiempirical model in molecular dynamics simulations, whereas the intrinsic gas-phase energy for the reaction is determined at a higher level of theory. Thus, the total energy (and free energy) of the system can be expressed as follows:

$$E_{\mathrm{tot}} = E_{\mathrm{QM}}^{\mathrm{HL}}(\mathrm{gas}) + E_{\mathrm{QM/MM}}^{\mathrm{LL}}(\mathrm{enzyme}) + E_{\mathrm{MM}}(\mathrm{enzyme}) \quad (6)$$

A similar energy separation has also been proposed by Morokuma and co-workers.[96,134,135] This approach has recently been used by Marti et al. in the study of chemical reactions in solution and for dehalogenase enzyme reactions,[136] and a previous application by Thomas and Field showed that the associative vs dissociative nature of the mechanism for the hypoxanthine–guanine–xanthine phosphoribosyltransferase reaction can change when semiempirical energies are substituted by high-level ab initio results.[137]

In closing this section, we point out that the reparametrization process to improve the accuracy of semiempirical models is usually carried out for the model reactions in the gas phase[13,116,120,138] and for bimolecular hydrogen bonding interactions between the solute (substrate) and solvent (amino acid functional groups).[132,139] These are the intrinsic properties of the QM/MM Hamiltonian that we correct to achieve the required accuracy for studying enzymatic reactions. Alternatively, one can reparametrize exchange and correlation functionals in DFT models. Then, the QM-SRP/MM potential is used in subsequent molecular dynamics simulations for the reaction both in water and in the enzyme. Unlike some empirical calibration procedures, this can be (and usually is) used with no further adjustments in molecular dynamics simulations to obtain the free energy of activation of the aqueous reaction for comparison with experiment. We consider this step, that is, the

agreement between experiment and the computed (rather than fitted) solvent effects on the free energy of activation, as validation of the QM/MM potential for describing substrate–solvent interactions. In contrast, if the potential function has been fitted to obtain the free energy of activation for the aqueous reaction by adjusting parameters directly affecting the barrier height, such as the resonance integral between VB states, solvation effects may not be adequately treated, which can affect the interpretation of solvation or desolvation effects in enzymatic catalysis. By determining solvation effects by means of free energy simulations for the aqueous reference reaction, we can study enzymatic processes more reliably.

## 2.3. Free Energy Simulations

A key quantity in studying enzymatic reactions is the free energy difference, $G^{\ddagger}(T)$, in eq 5. Equation 3 shows that this is primarily determined by computing the potentials of mean force along the reaction coordinate for the reactions in water and in the enzyme. Two methods are generally used, the umbrella sampling technique[30,140] and the free energy perturbation (FEP) theory;[141,142] these methods have been reviewed previously.[45,143]

Although FEP theory is exact,[141] in practical FEP applications,[45,142,144] the "perturbation" of the environment (enzyme and solvent) by the structural changes of the substrate from the reactant state to the next sampled point on the reaction path leading to the transition state is assumed to be small. In an extreme version, the free energy of activation can be determined by only considering the interactions between the substrate and enzyme.

$$\Delta\Delta G^{\ddagger}_{\text{FEP}}(T) = -RT\ln\left\langle e^{-\beta[\Delta E_{\text{ES}}(\text{TS}) - \Delta E_{\text{ES}}(\text{RS})]}\right\rangle_{\text{RS}} \quad (7)$$

where $E_{\text{ES}}(\text{TS})$ and $E_{\text{ES}}(\text{RS})$ are interaction energies between the substrate (including the residues participating in bond forming and breaking) and the enzyme at the transition state (TS) and reactant state (RS). In general, the "perturbation" from the reactant state to the transition state is, in fact, too large to have good convergence in one simulation. Thus, eq 7 is separated into multiple simulations that gradually transform ("mutate") the system from the reactant state to the transition state to minimize the convergence problem. Nevertheless, if the enzyme conformation change is significant during the catalytic process, the computed free energy difference of eq 5 from umbrella sampling simulations (US) of the catalyzed and uncatalyzed reactions, $\Delta\Delta G^{\ddagger}_{\text{US}}(T)$, can be significantly different from that obtained from free energy perturbation calculations, $\Delta\Delta G^{\ddagger}_{\text{FEP}}(T)$. This is illustrated by eq 8, which recasts eq 7 as the difference between the intrinsic binding (solvation) free energies (see Scheme 2)[210,243] of the substrate reactant state E′•S and transition state E″•S‡:

$$\Delta\Delta G^{\ddagger}_{\text{FEP}}(T) = \Delta G_{\text{ES}}(\text{E}'' \bullet \text{S}^{\ddagger}) - \Delta G_{\text{ES}}(\text{E}' \bullet \text{S}) \quad (8)$$

where the intrinsic binding free energy is defined in Scheme 2, which has the same meaning as that described by Jencks.[210,243] In eq 8, we have emphasized that the free energies of binding for the transition state and reactant state are determined by different enzyme conformational substates (E′ and E″) corresponding, respectively, to the reactant and the transition state being bound in the active site. The differences in structure and electronic properties between S and S‡ induce different enzyme conformations, denoted by E′ and E″,

respectively.[145] Typically, the FEP calculations do not lead to the same conformations of the free enzyme (enzyme with substrate unbound) when simulations start from E′•S and E″•S‡.[43,44] This is especially true when these calculations are performed only to determine the electrostatic component of the free energy of solvation by annihilating the "solute" charges while keeping the van der Waals spheres of the substrate (solute) fixed in the active site.[6,45–47] This "small" computational detail is often ignored in some discussions, but the presence of the van der Waals spheres prevents the protein from relaxing to its apo-enzyme conformation, **E**, and water molecules from filling in the cavity occupied by the substrate skeleton. Thus if free energy perturbation calculations are performed only at the structures corresponding to the reactant and transition state of the substrate, where there is insufficient overlap of the enzyme conformational space between the two states,[146] the computed free energy of activation may not include the free energy change due to the difference in the enzyme conformations.[43,44]

In contrast, the umbrella sampling technique provides a direct estimate of the relative probability of finding the reaction system at the reactant position along the reactant coordinate and at the transition state position; this estimate includes both the structural variations of the substrate and dynamic conformational changes of the enzyme along the reaction coordinate. Thus, it provides the most accurate estimate of $G^{\ddagger}(T)$ for the given potential energy surface.

Although eq 8 is not recommended to compute the reduction of free energy barrier in catalysis, it can provide important insights into the origin of catalytic power by comparing to the results from umbrella sampling simulations. If we approximately separate the total binding free energy of the substrate by the enzyme, $E$, into a free energy term, $G_{PP}(E')$, due to the enzyme conformational change induced by substrate binding and an intrinsic binding term, $G_{ES}$-$(E'\bullet S)$, of the substrate by this distorted protein configuration, we obtain the following expression (Scheme 2):

$$\Delta G_{M}(E' \bullet S) = \Delta G_{PP}(E') + \Delta G_{ES}(E' \bullet S) \quad (9)$$

A similar decomposition can be made for the transition state, $E''\bullet S^{\ddagger}$, but we denote that the enzyme occupies a conformational substate, $E''$, that may be different from that in the Michaelis complex. This free energy decomposition allows eq 5 to be rewritten as follows:

$$\Delta\Delta G^{\ddagger} = [\Delta G_{PP}(E'') - \Delta G_{PP}(E')] + [\Delta G_{ES}(E''\bullet S^{\ddagger}) - \Delta G_{ES}(E'\bullet S)] = \Delta\Delta G_{PP}^{\ddagger} + \Delta\Delta G_{ES}^{\ddagger} \quad (10)$$

The difference in free energy of activation can be directly computed from umbrella sampling simulations, $\Delta\Delta G^{\ddagger} = \Delta\Delta G_{US}^{\ddagger}$, whereas FEP calculations yield more closely the difference in intrinsic binding free energy between the reactant and transition state, $\Delta\Delta G_{ES}^{\ddagger} = \Delta\Delta G_{FEP}^{\ddagger}$. Consequently, if we rearrange eq 10, it can provide information on the contribution due to the change of the enzyme conformation upon the decrease (or increase) in the activation barrier of the enzymatic reaction:

$$\Delta\Delta G_{PP}^{\ddagger} = \Delta\Delta G^{\ddagger} - \Delta\Delta G_{ES}^{\ddagger} = \Delta\Delta G_{US}^{\ddagger} - \Delta\Delta G_{FEP}^{\ddagger} \quad (11)$$

The expression after the second equal sign tells how each quantity is computed.

Such computational analyses have been carried out for the decarboxylation reaction catalyzed by orotidine 5′-phosphate decarboxylase (ODC).[43,44] By umbrella sampling, it was estimated that $\Delta\Delta G^{\ddagger}_{PP} + \Delta\Delta G^{\ddagger}_{ES} = -22 \mathrm{kcal/mol}$, whereas FEP calculations yielded a value for the intrinsic binding free energy $\Delta\Delta G^{\ddagger}_{ES}$ equal to –2 kcal/mol. Consequently, the change in the internal free energy of the enzyme–solvent environment is about –20 kcal/mol in going from the reactant structure of the substrate to the transition state. The large free energy contribution from the enzyme itself on catalysis, not directly originating from protein–substrate interactions that stabilize the transition state structure, is attributed to a strain induced in the enzyme by substrate binding, which is subsequently relieved at the transition state, which has more charge delocalization.

### 2.4. Modeling the Michaelis Complex as the Initial Condition for Simulations

Another issue that is critical to all computer simulations of enzymatic reactions but has not received much attention is the construction of a model for the Michaelis complex; this is typically based on X-ray crystal structures. An important issue arises because, except in a few rare cases, the X-ray structures generally do not have their native substrates present because they would undergo rapid chemical transformations. (Instead they often have an inhibitor present or an empty active site.) In other cases, the crystal may have different quaternary structure (e.g., monomer, dimer, tetramer) than the active form of the enzyme in solution. Sometimes, there are two or more structures of a given enzyme that differ in binding partners or crystallization conditions, and even in the same structure, the ligand or cofactor(s) can have multiple locations.[147] Typically, one has to rely on a closely related substrate or transition state analogue inhibitor complex structure, if one is lucky, and manually dock the real substrate in the active site. Then, longtime molecular dynamics simulation is carried out in the hope of equilibrating the system to an active form for catalytic reactions. However, the time scale available for computer simulations, on the order of about 10 ns, is still much smaller than the physiological time for substrate equilibration. Therefore, the computational results are directly coupled to the actual structures used in the simulation, even if the potential functions have been validated and the computation has been carried out for as long as currently possible.

The consequence of choosing an X-ray structure to be used to obtain initial conditions for the simulation has been examined for two systems,[148] namely, the proton and hydride transfer reactions catalyzed by acyl-CoA dehydrogenase (ACAD)[138,149] and xylose isomerase (XyI),[150,151] in which the initial X-ray structure chosen to model the corresponding enzyme reaction was found to be in a significantly less reactive conformation than a second choice made later. ACAD constitutes a family of nine members that are optimal for different lengths of the substrate side chain.[152] For the human medium-chain ACAD (MCAD) to be modeled, the wild-type enzyme structure was determined in the absence of substrate, whereas the double mutant (Glu376Gly/Thr255Glu), designed to mimic the activity of the wild-type enzyme, contains an *n*-octanoyl-CoA substrate. A third option was to use the MCAD from pig liver mitochondria. In the first calculation, a decision was made to use the double mutant structure by changing back the mutated residues. Then,

in a second study, the butyryl ACAD (BCAD, an older name for short-chain acyl-CoA Dehydrogenase, also called SCAD) structure complexed with acetoacetyl-CoA was used. The computed potential of mean force for the first calculation has barriers, respectively, 13 and 17 kcal/mol higher for the proton and hydride transfer steps than those in the second calculation. Djordjevic et al. compared the X-ray structures of BCAD and MCAD and found that the active sites near the $C_\alpha$–$C_\beta$ and FAD regions align almost perfectly with a root-mean-square deviation of 0.2 Å.[153] The main difference in these two calculations is entirely due to the side-chain conformation of Arg256 (MCAD numbering), which is found to form an ion pair with the catalytic base Glu376, lowering its basicity. In BCAD, the guanidinium unit is flipped by 180°, occupying essentially the same cavity, but it is no longer directly hydrogen bonded to Glu376. PMF calculations using this conformation in MCAD resulted in a profile similar to that found in BCAD,[149] while in the meantime, a new crystal structure captured this conformation.[154] This study illustrates that relatively small structural variations can have large effects on a computed PMF. Thus, it is essential to compare computational results with experimental data on structures, mutations, and energies to the greatest extent possible.

The case of XyI illustrates a different structural issue in constructing the initial configurations for enzyme modeling; in particular, it is a case where the equilibrium structure from transition state analogue binding may differ from the transition state configuration derived during the enzymatic reaction, which begins from the Michaelis complex. A number of XyI structures with the substrate D-glucose or transition state analogues have been determined.[147,155–159] Despite very strong binding by the inhibitor, which can potentially induce large protein conformational changes, Petsko and co-workers showed that the overall structural difference between the inhibitor complex and the apo-enzyme had a very small $C_\alpha$ RMS deviation of 0.27 Å, suggesting such a global comparison of structures was insufficient for characterizing active-site interactions.[147,156] Two structures are compared in the present discussion, the D-glucose complex (1XYB) determined by Whitlow et al.[159] and the inhibitor complex (2GYI) determined by Allen et al.,[147,156] which leads to a small difference in the proposed coordination sphere to the Mg2 ion (i.e., the second Mg ion cofactor), which is a "mobile" ion during the reaction (Scheme 3). Both mechanisms begin with the same initial Michaelis complex structure, but the intermediate prior to the hydride transfer step, which is produced by deprotonation of the 2-OH group, has different coordination interactions with Mg2 (Scheme 3). Based on the 2GYI structure, in which Asp254 and Glu185 have very close contacts and, it was assumed, form a hydrogen bond from a protonated Asp254, Mg2 was suggested to coordinate with two water molecules. On the other hand, in the 1XYB mechanism, Asp254 maintains one ligation to Mg2, which has only one water ligand. PMF calculations by umbrella sampling using a combined QM/MM potential that has been validated for model reactions in the gas phase were performed.[150,151] The 2GYI mechanism has a barrier and reaction free energy that are 5 and 12 kcal/mol higher, respectively, than the 1XYB pathway.[148] The latter was found to be in better agreement with experiment. We attributed the difference to an imbalance of charges when Asp254 lost its coordination in the first case, whereas there is no net charge loss or gain in the Mg2 ligand sphere along the reaction path. The structural difference also favors stabilization of the transition state by Lys182 in the 1XYB configuration. This

example again illustrates the need for carefully examining the structures used in enzyme simulations. It is especially important to keep in mind that the crystal structures are observed under equilibrium conditions, typically at very low temperature; thus, even when the reactant or transition state analogues are very similar to the real substrate, the crystal structure does not necessarily correspond to the reactive form.

In concluding this section, we return to the study of the ODC decarboxylation reaction, for which numerous structures complexed with a variety of reactant, product, and transition state analogue inhibitors for enzymes from all kingdoms of life have been determined.[6,161–165] Despite this diversity, the active site structures are remarkably similar, including those for a number of mutants. Careful comparison of the simulated structures from the work of Wu et al.[6] shows that the transition state configurations are very similar to the X-ray structure complexed with 6-aza-UMP, a transition state analogue, and other ligand-bound structures.[44] The average locations of the phosphate group and the ribosyl ring are nearly superimposable on the X-ray structure. But, the reactant state conformations show distorted substrate structures and migrations of Lys72, Asp70, and other charged residues by as much as 1.5 Å from the "equilibrium" transition state conformations, yet still keeping the ribosyl phosphate location in the binding pocket. The agreement with the experimental X-ray structures is a main reason for the good results obtained in free energy simulations.[6,44] It would be interesting to compare structures used in different simulations that resulted in different conclusions on the origin of the ODC catalysis.[6,44,46,166]

## 2.5. Reaction Coordinates

Both the two critical quantities in eq 1 depend on the choice of the reaction coordinate, $q$. For a multidimensional condensed-phase system such as the active site of an enzyme-catalyzed reaction, it is not always clear how best to choose the reaction coordinate. Most work uses a simple function of valence coordinates (e.g., geometrical parameters such as a dihedral angle or the difference between the making and breaking bond lengths),[11,13,36,55,167–170] whereas other studies employ a collective bath coordinate, as in Marcus theory:[29,32,68–70,73,171,172,183]

$$\Delta E = V_R - V_P \quad (12)$$

where $V_R$ and $V_P$ are, respectively, the energy of the diabatic reactant electronic state and the diabatic product electronic state.[60,68] In many cases, it is possible that both definitions of the reaction coordinate are adequate.

For systems for which little is known about the details of the reaction path, a number of methods have been developed for finding the best description of the reaction coordinate. Examples of such methods include reaction path searching[173–175] and transition path sampling.[176–179] Nudged elastic band algorithms are another alternative.[180,181] One can also use umbrella sampling along an unoptimized reaction coordinate to generate a transition state ensemble and then average over an ensemble of steepest descent paths originating from this ensemble.[12,13]

A reaction coordinate can be validated by determining the dynamic recrossing factor, $\Gamma(T)$, of eq 2. A good choice of the reaction coordinate followed by optimization of the location of the transition state hypersurface as a function of position along that coordinate will result in a recrossing transmission coefficient close to unity. On the other hand, a poor choice of the reaction coordinate or the transition state will require more effort in computing $\Gamma(T)$, which would have a very small value.

Despite the fact that the use of geometrical valuables to define the reaction coordinate can be justified as noted above, it has sometimes been suggested that this definition for reactions in solution or in enzymes may not provide adequate sampling of the solvent–protein configurations because these slower "environmental" coordinates must respond to the "faster" changes in the solute internal degrees of freedom along the reaction coordinate.[32,182] One might even argue that, since both solvent and solute coordinates must respond to the bias of the energy gap coordinate when eq 12 is used as the control variable in molecular dynamics simulations, such a collective coordinate is a superior reaction coordinate and should yield a more accurate description of the reaction. However, studies where potentials of mean force have been computed as a function of both the geometrical and the energy gap reaction coordinate for reactions in solution suggest that the computed free energies of activation are very similar from these two approaches, even for proton-transfer reactions in water.[68–70,183] The relationship between the two kinds of reaction coordinates has been analyzed in terms of two-dimensional energy functions, where one dimension is a valence coordinate and the other is an energy gap.[183]

The sampling efficiency of the energy-gap reaction coordinate in simulations based on a geometrical reaction coordinate for the enzymatic reaction catalyzed by dihydrofolate reductase (DHFR) has also been analyzed.[122] The potential of mean force for the hydride transfer reaction has been determined using both the energy-gap reaction coordinate[73] and a geometrical coordinate defined as the difference between the distances of migrating hydride ion from the acceptor and donor carbon atoms, $z$.[122] In both calculations, the estimated recrossing transmission coefficients are very similar with a value of about 0.8–0.9, suggesting that both types of reaction coordinates are equally effective in describing this enzymatic hydride transfer reaction (we note that different potential functions are used in these two studies; however, this is not a problem in comparing sampling efficiency). This analysis is strengthened in Figure 1, which depicts the average energy gap, $E(z)$, as a function of the geometrical reaction coordinate for the DHFR reaction. Using the configurations generated by umbrella sampling simulations along a geometrical coordinate, we have computed the energy differences between the reactant and product diabatic states, that is, the energy gap reaction coordinate, both including and excluding the change in intramolecular interaction terms. Figure 1 shows the computed energy gap as a function of the geometrical reaction coordinate from the reactant to the product regions. We found that all regions of the energy gap coordinate were included in the configurational space sampled by using a geometrical reaction coordinate. Therefore, umbrella sampling calculations that employ a geometrical reaction coordinate can provide solvent–enzyme configurations that span the same range of substrate–enzyme interaction energies as those in simulations using an energy-gap reaction coordinate. There is no particular advantage of using the energy-gap

coordinate, at least with regard to sampling efficiency of the enzyme conformational subspace as measured by the range of enzyme–substrate interactions. In fact, it is expected that the effect is even smaller for heavy-atom transfer reactions.

Since the use of a geometrical variable as the reaction coordinate is particularly instructive and intuitive for chemists and biochemists to describe the mechanism of chemical reactions and enzymatic processes, it is often used in free energy simulations. Use of this reaction coordinate also allows convenient analysis to compare specific structures with those obtained from spectroscopic and X-ray diffraction experiments, even when an ensemble of reactant and transition state structures is considered.

## 3. Mechanisms of Enzymatic Reactions

Studies of enzymatic reactions show that natural selection has developed many ways for lowering the quasithermodynamic free energy of activation (eq 1).[7] In the following, we do not aim to make an exhaustive survey, but rather we discuss the structures, free energies, and reaction mechanisms of selected enzymes that are well understood through computation and experiment. Computational studies can be roughly grouped into two types, those involving only energy optimizations for the stationary structures along the reaction path, either for model systems or in the presence of the enzyme, and those determining the potential of mean force and free energy of activation for the enzymatic reaction. Although the former can be informative in oxidation–reduction processes at transition metal centers, they do not include the effects of enzyme dynamics, which are essential for understanding catalysis. Consequently, they are generally not included in the present discussion. Our aim here is to highlight some of the key features and different mechanisms that enzymes use to lower the free energy barrier (Table 1).

### 3.1. Transition-State Stabilization by Electrostatics Including Hydrogen Bonding

Transition state stabilization is a central concept in understanding enzyme catalysis; for example, it has served as the basis for the design of transition state analogue inhibitors and for eliciting catalytic antibodies.[1,7,32,36] Analyses of simulation results are providing a detailed understanding of how the free energy of activation is lowered by the enzyme, including a delineation of the enzyme structure and its flexibility. Hydrogen bonding and other electrostatic effects are often found to dominate the stabilization of the transition state, although other factors also contribute, such as desolvation and the change in a pre-organized enzyme environment leading to stronger interactions for the transition state than the reactant state.

One of the enzymes in which electrostatic effects are dominant is enolase, a glycolytic enzyme that catalyzes the abstraction of a proton from the carbon acid ($pK_a > 32$)[184] of 2-phospho-D-glycerate (PGA) substrate by use of a weak-base lysine residue to produce phosphoenolpyruvate ($RCH{=}CO_2^{2-}$). Enolase is a representative member of a large class of enzymes called the enolase superfamily,[185,186] and it must overcome the large thermodynamic barrier for the reaction, corresponding to the $pK_a$ difference between the carbon acid and lysine. The active site consists of two $Mg^{2+}$ ions, both of which are coordinated to PGA: one forms a bidentate ligation to the carboxylate group, and the other is

bound to the anti lone pair of one of the carboxylate oxygen atoms, as well as to one of the phosphate oxygens (Figure 2).[186] Model calculations have led to estimates that the energy to achieve a nearly thermoneutral reaction in the enzyme is about 290 kcal/mol relative to the gas-phase reaction and is about 25 kcal/mol in aqueous solution, as determined from the p$K_a$ values. The PMF for the proton abstraction reaction was computed[120] using a combined AM1/CHARMM22 potential, which yielded a free energy of activation of 14.4 kcal/mol when quantum effects on nuclear motions are included. The predominant contribution to lowering the barrier for the proton-transfer reaction, which is about 56 kcal/mol as estimated for the bimolecular reaction at the Michaelis complex configuration in the gas phase, arises from electrostatic interactions of the doubly charged enolpyruvate dianion group with two $Mg^{2+}$ ions, relative to the interactions of the singly charged carboxylate ion, PGA, in the Michaelis complex. Here, the metal ions do not directly interact with the base for the proton abstraction step nor stabilize the leaving group in the dehydration step.

The enolase-catalyzed reaction has been studied by Liu et al.,[187] who, using a combined B3LYP/GROMOS model, first located the minimum energy pathways and then determined the free energy barriers both for the α-proton abstraction of PGA by Lys345 and for the removal of the β-hydroxyl group from the enolic intermediate assisted by Glu211, which has been identified experimentally.[188] These authors also found that the two metal ions play a key role in providing electrostatic stabilization during the formation of the enolpyruvate intermediate. However, the metal ions strongly disfavor the dehydration step due to an opposite charge migration away from the $Mg^{2+}$ ions. Yet, the placement of key ionic residues in the enolase active site allows for opposite charge flows in the proton abstraction and dehydration steps without making the overall reaction barrier too high.

Hydrogen bonding interactions are found to play a critical role in transition state stabilization for the dephosphorylation reaction of a phosphotyrosine substrate catalyzed by the low-molecular weight bovine protein tyrosine phosphatase (BPTP). The BPTP reaction is of particular interest, in addition to its biological importance, because the phosphate hydrolysis reaction is catalyzed purely by a nucleophilic substitution mechanism without the assistance of metal ions,[189,190] and the mechanism is shared by the catalytic domain of human PTP1B.[191,192] Structural and biochemical studies demonstrated that Cys12 is the nucleophile; it forms a phosphothiol ester intermediate, which is hydrolyzed by water. Each of the two steps involves a Walden inversion at the phosphorus center, in conjunction with the nucleophilic attack. The free energy reaction profiles for a phosphotyrosine dianion and for a phosphotyrosine monoanion have been determined using a combined QM/MM potential, employing a semi-empirical AM1/MNDO/CHARMM22 force field in umbrella sampling simulations. The free energy of activation was computed to be 14 kcal/mol, in accord with experiment.[193]

More importantly, analyses of the simulation results revealed that a delicate balance of hydrogen bonding network and structural organization of the BPTP active site is critical to the nucleophile Cys12 activation, substrate binding, and transition state stabilization (Figure 3). In fact, this system provides an excellent example, illustrating the significance of correlating structural information from computation and X-ray crystallography with enzyme activity to understand catalysis.[193,194] The phosphate binding site of PTP is characterized by

the signature loop with a sequence of CXX-NXXR(S/T), where X can be any residue. The nucleophile Cys12 is stabilized by hydrogen bonding interactions from the side chains of Asn15 and Ser19 and the amide group of Ser19, making it a thiolate ion by lowering its p$K_a$[195] and positioning it in the center of the binding loop perfectly suited for the in-line nucleophilic attack (Figure 3).[193] The backbone amides (XXNXX) along with the side chain of Arg19 constitute the core structure for phosphate dianion binding, providing three hydrogen bonds to each of the three nonbridging phosphate oxygen atoms (Figure 3). As the nucleophilic substitution reaches the transition state, the extrusion of the nonbridging oxygens to take the equatorial positions of the trigonal bipyramidal transition state brings them closer to the phosphate binding loop, evidenced by average reductions in hydrogen bond distance by 0.05 to 0.1 Å. Energy calculations suggest that this change, enforced mechanistically by the Walden inversion of configuration, leads to transition state stabilization by –4.6 to –6.2 kcal/mol relative to the reactant state binding. Interestingly, similar trends have been observed in the X-ray structures complexed with $VO_4^{2-}$, a transition state analogue, in which the reduction of hydrogen bond distances is 0.12–0.18 Å in comparison with the structures when the phosphate substrate is present.[196,197] Of course, when comparison is made with the X-ray interatomic distances, only the trends of changes are of special interest in view of the intrinsic uncertainties in structure refinements. The Walden inversion enforced hydrogen bonding stabilization is possible in the enzyme because the $(X)_5$-loop is encompassed by a second layer of loop hydrogen bonds, making its structure less flexible, whereas in aqueous solution, water molecules can easily adjust their positions.

PTP has been studied by a number of groups. Hillier and co-workers determined the reaction path using a combined PM3/MM potential for the dephosphorylation reaction.[198] Peters et al. studied substrate–PTP binding and its effects on protein motions through molecular dynamics simulations,[199,200] while Åqvist and co-workers carried out extensive simulations of substrate binding and the reaction mechanism using an EVB potential.[201–204] These studies also showed the important roles of the phosphate binding loop on stabilizing the transition states both for the thiolphosphate intermediate and for the subsequent hydrolysis, and the proton transfer from Asp129 to the phenoxide leaving group is concerted with the nucleophilic attack by Cys12.[204]

Another enzyme for which electrostatic effects are dominant is triosephosphate isomerase (TIM), which catalyzes the conversion of dihydroxyacetone phosphate (DHAP) to (R)-glyceraldehyde 3-phosphate (GAP).[4] The reaction barrier for the enzymatic process is lowered by as much as 13 kcal/mol relative to that of the uncatalyzed reaction in water using QM methods ranging from semiempirical (AM1-SRP) to DFT in QM/MM potentials[118] to the EVB approach.[205] The calculations by Cui and Karplus involve energy optimizations of the enzymatic reaction, and it was found that although short hydrogen bonds occur during the reaction, they do not contribute to catalysis. Overall, the enzyme employs charged and polar groups to stabilize the reaction intermediate, with Lys12 making the most important contribution. Guallar et al. reported a combined QM/MM geometry optimization using DFT and a newer TIM–DHAP crystal structure.[41,206] The authors found that it is the phosphate monoanionic form of the DHAP substrate that is preferred in the catalytic process,

exhibiting a barrier height 4.5 kcal/mol lower than that of the dianion substrate for the rate-limiting proton abstraction. However, most computations have been carried out by geometry optimization,[207] and it would be interesting to determine the effects of enzyme dynamics and conformational fluctuations on the reaction pathways from free energy simulations. The recrossing transmission coefficient for the proton abstraction process has been estimated in various ways as 0.43,[71] 0.69,[168] or 0.53,[20] but it is not clear whether this is a diagnostic for significant effects of dynamical interactions in the active site. Interestingly, experimental work has shown that the large catalytic power exhibited by TIM can be attributed to the preferential binding of the nonreacting phosphate group in the transition state as compared to the reactant; this binding was estimated to be 14 kcal/mol in the transition state of the enzyme-catalyzed enolization reaction.[208] Complete computational studies of the contribution due to intrinsic binding of this group have not been performed, although Cui and Karplus[20] reported large stabilization of the phosphate by polar and charge interactions, made model systems in which the phosphate group was replaced by a methoxy group, and discussed this result in the light of their simulations.

### 3.2. Desolvation and Reactant State Effects

Often, it is not straightforward to dissect the specific contributions to the overall barrier reduction. In principle, the free energy barrier of the catalytic step ($E' \cdot S \rightarrow E'' \cdot S^\ddagger$) can be reduced in the enzyme relative to the same reaction ($S \rightarrow S^\ddagger$) in water both by transition state ($E'' \cdot S^\ddagger$) stabilization and by reactant state ($E' \cdot S$) destabilization, but controversies and passionate arguments have surrounded this topic for a long time.[1,209–211] A detailed understanding of various contributing factors to catalysis may begin with the study of solvent effects on the uncatalyzed reaction in water. Thus, it is very helpful to investigate the same reactions in *all three environments*—in the gas phase, which yields information on the intrinsic reactivity of the chemical process; in water, which provides solvation effects; and in the enzyme, which is relevant to catalysis. Technically, the study of the gas-phase reaction provides validation of the potential energy function; the simulation of the reaction in aqueous solution further justifies the potential energy function for describing solute and aqueous solvent interactions; and finally, the calculation in the enzyme active site allows analyses of factors contributing to catalysis in an unbiased way. (One could also consider other possibilities, such as reactions in hexadecane, to simulate the uncatalyzed reaction in a hydrophobic environment to mimic certain active sites, but this has apparently never been done.)

One example that involves both desolvation and transition state stabilization contributions to lowering the barrier height of the reaction is haloalkane dehalogenase (DhlA),[212] a dimeric enzyme that catalyzes the removal of chloride ion leaving group from 1,2-dichloroethane (DCE) substrate, a hydrophobic compound that is carcinogenic and an environmental pollutant with very long lifetime in soil and water.[213] The enzymatic reaction involves two steps, first a nucleophilic attack by Asp124 to yield an alkyl ester covalent intermediate and second a hydrolytic cleavage of the ester bond by a water molecule that is activated by a $H_2O$–His289–Asp260 triad. It is fortunate that X-ray structures complexed with the DCE substrate, the ester enzyme covalent intermediate, and the product chloride ion have all been

determined, because this provides us with a rare case with structural information on all key reaction intermediates in the enzyme for comparison with computational results.[212,214–216]

The potentials of mean force for the enzymatic reaction of DCE in DhlA and for a model reaction of DCE with acetate ion in water have been determined using an AM1-SRP/MM potential that was originally fitted to reproduce ab initio results in the gas phase at the MP2 level by Bruice and co-workers.[116] All molecular dynamics simulations were performed using periodic boundary conditions for a system consisting of 29 540 atoms, of which 15 atoms from DCE and Asp124 are treated quantum mechanically.[169] The energy barrier for the gas-phase reaction is 21.3 kcal/mol from the ion–dipole complex to the transition state using the AM1-SRP model, corrected to the best theoretical result at the G2 level of theory.[217] The PMFs were determined along the mass-weighted asymmetric stretch coordinate involving the nucleophile, the substrate, and the leaving group, and the free energies of activation were found to be 26.7 and 15.8 kcal/mol for uncatalyzed and enzyme-catalyzed reaction, respectively,[169,217] in good accord with the corresponding experimental values of 28.2 (this is an extrapolated barrier from higher temperature measurements as typically done for slow spontaneous reactions[2,5]) and ~15.3 kcal/mol. Thus, the enzyme DhlA lowers the activation barrier by ~11 kcal/mol from free energy simulations, compared with the experimental $\Delta G^{\ddagger}$ of 13 kcal/mol. We present these specific values to illustrate the importance of parametrizing the potential energy functions to be used in simulation studies of enzymatic reactions against only the gas-phase reaction, to obtain insights into the origin of enzyme catalysis.

Relative to the gas-phase ion–dipole complex between DCE and acetate ion, solvent effects increase the free energy barrier for the $S_N2$ reaction in water by 5.4 kcal/mol,[169] whereas the DhlA reduces the barrier height by 5.5 kcal/mol, giving rise to the net 10.9 kcal/mol reduction in $\Delta G^{\ddagger}$. It is well-understood that the large aqueous solvent effect on $S_N2$ reactions is due to greater solvation of the charge localized reactant state than the charge dispersed transition state.[55] However, this still does not tell us that the overall barrier reduction of 10.9 kcal/mol can be separated into contributions of 5.4 kcal/mol from desolvation and 5.5 from transition state stabilization because the enzyme could potentially have an even greater "solvation" stabilization of the reactant state at the Michaelis complex than aqueous solvent does on the ion–dipole complex. To achieve this goal, we determined the free energies of solvation for the transfer of the reactant state and the transition state into water and into the active site.[218] Figure 4 illustrates the relative free energies of solvation; here, we have used the word "solvation" in a generalized sense to denote substrate–enzyme interactions. In the figure, the Michaelis reaction precursor, the QM region in E′•S, has been labeled RS to denote reactant state. As expected, the RS is more stabilized than the TS by 5.8 kcal/mol in water, in accord with results obtained by PMF simulations.[169] In contrast, the enzyme provides greater stabilization of the TS than the Michaelis complex (RS in Figure 4) by −4.3 kcal/mol, also consistent with the PMF results.[169] Moreover, the enzyme active site has much weaker interactions with the reactive species (DCE and Asp124) than the aqueous solvent does (−74 vs. −45 kcal/mol), as determined by comparing the absolute solvation free energies (Figure 4). This suggests that the DhlA active site provides poorer solvation than the aqueous environment for acetate ion and DCE.

This energetic conclusion is further confirmed by qualitative results from analyses of the reaction dynamics in the enzyme and in aqueous solution. Using a reactive flux approach, Nam et al. have determined the recrossing transmission coefficients for the catalyzed and uncatalyzed reaction; they are 0.53 and 0.26, respectively, suggesting that the dominant contribution to catalysis is due to the reduction in free energy barrier.[169] The results show that the choice of the geometrical reaction coordinate is very good since the recrossing transmission coefficients are both close to unity. The reaction dynamics was characterized by computing the autocorrelation function (ACF) of the fluctuating forces on the reaction coordinate at the transition state, which provides information on the nature of substrate–environment interactions (Figure 5) through the generalized Langevin equation.[169] It is clear from Figure 5 that the dynamical interactions that dictate the recrossing events in water are due to electrostatic and hydrogen bonding interactions because the computed ACF is characteristic for solvation of ions in water with fast (50 fs) and slow (2 ps) relaxations and by analysis of energy components.[169] In DhlA, analysis of energy components shows no evidence of strong electrostatic coupling with the enzyme. The rapid oscillation, which is also present for the reaction in water but it is overwhelmed by solute–solvent hydrogen bonding, can be attributed to the intramolecular symmetric vibrational mode by examining its power spectra through Fourier transform.[169] Combining the results from computed free energies and the friction kernels of reaction coordinate dynamics, we conclude that both desolvation and transition state stabilization contribute to barrier reduction in DhlA catalysis and that each factor contributes about 5.5 kcal/mol.

The free energies and dynamical recrossing transmission coefficient for the same DhlA reaction have also been determined by Soriano et al.,[170,219] and their results reaffirm the conclusions of ref 169. On the other hand, using an EVB potential, Olsson and Warshel reached the conclusion that "the transition state is 'solvated' by the protein more than in the reference solution reaction". Interestingly, in an earlier paper on the same system,[220] Shurki et al. concluded that "the electrostatic solvation effects *increase* (original italics) the intramolecular barrier for the $S_N2$ reaction but it does so in a less pronounced way in the enzyme than in water" (other researchers describe this phenomenon as desolvation), which appears to be contradictory to the newer findings. Nevertheless, Olsson and Warshel attributed their results to the pre-organization of the protein–solvent coordinates,[47] and they stated that this is fundamentally different than the "frequently proposed" desolvation mechanism.[169,217,220]

These authors determined the "solvation" free energies for species corresponding to the ion–dipole complex (called the reactant state in a solvent cage) and the transition state in water and in the active site of DhlA.[47] They obtained free energies of solvation of −78 and −55 kcal/mol for RS and TS in water, and −96 and −81 kcal/mol in the enzyme. Since the "solvation" free energy of the reactant state is much greater in the enzyme than in water, it was concluded that the origin of catalysis must be due to transition state stabilization. Aside from the observation of an unrealistically huge "solvation" of a carboxylate group in the enzyme active site, which would yield an unprecedented p$K_a$ of −8 for Asp124, the difference in free energies of solvation and the barrier for the reaction in water does not yield reasonable barrier for the reaction in the gas phase. Olsson and Warshel obtained a

difference of 23 kcal/mol in solvation free energy between the reactant state and the transition state, which is nearly identical to the computed barrier (24.2 kcal/mol) for the aqueous reaction;[47] this implies that the transition state and the "reactant state" (at the minimum configuration in water, $\langle R \rangle_{RS}^{w}$) must have similar free energies in the gas phase. They found that this "reactant state" at $\langle R \rangle_{RS}^{w}$ is 13 kcal/mol greater than the ion–dipole complex, the minimum in the gas phase (see footnote on p 15172 of ref 47). Thus, the free energy barrier, relative to the ion–dipole complex, for the reaction in the gas phase between acetate ion and DCE can only be 13–14 kcal/mol from the EVB potential, which is markedly different than the barrier height of $\Delta G_{gas}^{\ddagger} = 21 - 25 \text{kcal/mol}$ determined from a variety of high-level ab initio calculations including MP2 and G2 theories.[116,217,221–223] This discrepancy must be somehow absorbed in the parameters of the EVB potential by adjusting the $\varepsilon_{12}$ term to yield the desired free energy of activation in water.[47] Consequently, such parameter adjustments do not provide solvation effects directly from simulations. This is not a problem if one is only interested in knowing "catalysis", that is, the change in the barrier height from water into the enzyme active site,      $G^{\ddagger}$, but it can be problematic for interpreting the origin of the barrier reduction, especially when solvation and desolvation effects are considered.

The DhlA reaction has been studied by several other groups, utilizing energy minimization or molecular dynamics simulation of the reactant state.[47,116,169,217,220,223–229] Bruice and co-workers have focused on identifying enzyme configurations that are most suitable for the nucleophilic attack.[116,227] However, Shurki et al. suggested that these near attack conformations do not make important contributions to catalysis.[220]

An enzyme that employs both transition state stabilization and reactant state destabilization, induced by substrate binding, is chorismate mutase, which catalyzes what is formally a Claisen rearrangement of chorismate to prephenate in the biosynthesis of aromatic residues. The unimolecular process provides a nearly ideal case for understanding the origin of a "pure" enzyme catalyst, and thus, it has attracted numerous theoretical studies.[112,230–240] Electrostatic interactions stabilize the transition state, lowering the free energy barrier by several kilocalories per mole.[241] The substrate chorismate exists predominantly in a diequatorial conformation in aqueous solution. Upon binding, it is forced to adopt a diaxial conformation, which contributes about 5 kcal/mol to catalysis,[233] in agreement with the analysis of mutation results. This substrate conformation change, to position the 1–5 diene in a chairlike conformation, has been termed a "near attack configuration" (NAC). Bruice and co-workers found that nearly all chorismate mutase catalysis is due to the NAC effect,[112,234] and others have estimated this effect to contribute about 4 kcal/mol.[242] Warshel and co-workers used an EVB potential to analyze the importance of the NAC effect in the chorismate reaction and concluded that catalysis in chorismate mutase is by transition state stabilization and not the NAC effect.[235]

Another system that also attracted similar attention is the decarboxylation of OMP, which has been introduced in section 2.4, where the dominant contribution to the barrier lowering was attributed to the free energy released during the enzymatic process in going from highly strained enzyme conformational substates at the Michaelis complex, induced by substrate

binding, to the TS conformational substate, which is less strained.[6,43,44] This mechanism has been described by Jencks,[210,243] and this is a reactant-state effect. In this discussion, it should be pointed out that such a reactant-state destabilizing effect is not inconsistent with the fact that the overall binding of the substrate by the enzyme is favorable because specific substrate–enzyme interactions compensate for the "destabilizing" energy of the enzyme itself. A combined QM/MM potential used by Wu et al.[6] has been validated against the gas-phase and aqueous reactions,[244] and the solvation effects and enzymatic effects obtained from molecular dynamics simulations were found to be in good accord with experiments. An interesting finding from X-ray diffraction studies is that the Asp70Ala mutant appears to be still active as the OMP substrate is converted into UMP, where the catalysis was rescued by the presence of a chloride ion in the location of the wild-type Asp70. Free energy simulations were performed for the Asp70Ala mutant both with and without the presence of a chloride ion.[44] The PMFs shown in Figure 6 illustrate a gradual reduction of the free energy barrier from 38 kcal/mol for the uncatalyzed reaction to 30 kcal/mol for the Asp70Ala mutant, which is further lowered to 20 kcal/mol if the chloride ion is introduced in place of Asp70. The wild-type enzyme, which has the anion covalently linked to the enzyme, has a computed barrier of 15 kcal/mol. The gradual change of free energy barrier provides a further indication of the reliability of the computational procedure. It demonstrates the importance of an anion residue for protein distortion upon the substrate binding.

The ODC reaction was studied by Warshel et al. using an EVB potential in molecular dynamics simulations and free energy calculations using a Langevin dipole model, and they suggested that the rate enhancement is due to the TS stabilization rather than reactant state destabilization.[46] They attributed the difference between their conclusion and that of ref 6 to the selection of the reference reacting system and long-range electrostatic effects. In the work by Wu et al.,[6] the unimolecular reaction of methyl orotate in water was used and the OMP decarboxylation, also a unimolecular process, in the enzyme was compared. This procedure is the same as that used by Wolfenden and co-workers in their landmark studies.[5] Warshel et al. used an imaginary reaction of orotate$^-$ + LysH$^+$ → uracil + Lys + CO$_2$ as the reference reaction in water by placing an ammonium ion NH$_4^+$, which serves as a model for LysH$^+$, near the orotate leaving group, and they concluded that the ODC catalysis is entirely due to transition state stabilization by comparing solvation free energies of the reactant and transition state.[46] However, Wolfenden's experiments unequivocally demonstrated that the OMP decarboxylation is unimolecular both in solution and in the enzyme. Further, there is no evidence of counterion effects on the decarboxylation reaction in water. The reference reaction used by Warshel may contribute to the difference in interpreting the origin of ODC catalysis. When Lys72 is not restrained, significant conformational changes have been observed in going from the reactant state to the transition state, and this has been rationalized and compared with X-ray structures.[44] Yet, the ribosyl phosphate binding pocket was not altered.[44] A pedestrian inspection of the PMFs reported in ref 46 reveals that the product state, which is the transition state for the OMP decarboxylation reaction from all other studies,[6,166,244–246] is overly stabilized to a free energy only 1 kcal/mol (or 9 kcal/mol in another charge state) above the Michaelis complex. Such a strong stabilization of the

decarboxylation transient species, by as large as 10–16 kcal/mol from the "transition state",[46] may also contribute to the difference in interpreting the two computational results.

A number of mechanisms have been proposed for the ODC reaction.[46,166,244–247] Houk and Lee proposed a carbene intermediate based on ab initio electronic structure calculations at a time when the enzyme structures had not been determined.[244] A nucleophilic addition–elimination process was investigated by Kollman and co-workers.[248] Recently, Raugei at al. carried out ab initio molecular dynamics simulations of the ODC reaction along a fixed reaction coordinate using a DFT potential, but the simulation lasted for only 7 ps. These authors suggested that transition state stabilization was responsible for catalysis.[166] On the other hand, extensive studies by Wu and co-workers led to the proposal of reactant state destabilization.[245,246] In the study of the ODC reaction, which involves significant contributions from the change in enzyme conformation, it can be difficult to provide reliable results if the reaction coordinate was fixed in free energy calculations. Bruice and co-workers found that significant enzyme conformation changes take place as the decarboxylation reaction occurs,[247] a finding consistent with the mechanism of protein reactant state destabilization.[43]

A test of the proposed ODC mechanism is to explain the finding that mutations of residues that interact with the phosphate group, for example, Tyr217Ala mutation, which is at least 8 Å away from the decarboxylation site, increase the barrier height by 4.7 kcal/mol, but yet have small (~1 kcal/mol) effects on binding affinity.[2] None of the proposed mechanisms can explain this observation, except the enzyme reactant-state distortion (i.e., destabilization) mechanism, which is consistent with the experimental results.[43] Wu et al. predicted that if the OMP substrate were replaced by the 2′-deoxy analogue, the catalytic rate would be greatly reduced because it plays a key role in interacting with Lys72, a residue exhibiting large movement during the reaction.[6] This was confirmed by Miller et al. who found that the barrier increases by 4.6 kcal/mol.[249]

A recent study by Amyes et al. showed that the introduction of a phosphite dianion to a truncated OMP substrate without the $CH_2OPO_3^{2-}$ group increases the rate constant by a factor of 80 000 for the ODC-catalyzed reaction when it is absent.[160] This experiment provides strong support to the proposal that the release of protein distortion energy induced by substrate binding is the dominant contributor to ODC catalysis.[43,44] The binding of a phosphite dianion causes the enzyme to adopt a more distorted conformational substate that is relaxed by releasing a greater amount of protein distortion energy as the reaction reaches the transition state. This contributes to the lowering of the observed free energy of activation. It should be emphasized that such an induced conformational change is in the enzyme configuration itself, not in the reactive part of the substrate as originally proposed by Jencks.[6,210,243]

### 3.3. Enzyme and Substrate Conformational Dynamics

As seen in the ODC decarboxylation reaction discussed above, many enzymes undergo significant conformational changes during the enzymatic reaction. A certain degree of enzyme flexibility is undoubtedly essential for catalysis. Large-scale loop motions are known to be involved in catalysis as well as in providing a protected catalytic site while

permitting the substrate to enter and product to escape. In this section, we highlight the structural changes along the reaction pathways in two enzymes, xylose isomerase and dihydrofolate reductase.

Xylose isomerase (XyI) catalyzes the interconversion of D-xylose and D-xylulose and is one of the most widely used industrial enzymes for the production of more than a billion pounds of high-fructose corn syrup.[159] An important feature of the active site of XyI is a combination of two divalent ($Mg^{2+}$, $Co^{2+}$, $Mn^{2+}$) ions bridged by an aspartate residue;[250] a growing number of enzymes are now known to share this structural motif.[155,156] The overall enzymatic process is rather complex, involving the opening of the pyranose sugar ring, isomerization by a hydride transfer mechanism, and reclosing to form the cyclic sugar product.[159] X-ray structures have captured a number of intermediate configurations using various substrate and transition state analogue inhibitors. The key steps associated with the isomerization reaction are summarized in Scheme 3. The dynamic motions accompanying the chemical steps have been characterized by molecular dynamics simulations and combined QM/MM studies.[150,151,251–253] The initial deprotonation of the 2-OH group leads to a shortening of the distances between the two magnesium ions from 5.4 to about 3.6 Å stabilized by the formation of a second bridging ligand interaction from the substrate alkoxide ion. Following the hydride transfer from the C2 carbon to the carbonyl C1 position, the two $Mg^{2+}$ ions move apart again to an average value of about 5.0 Å because the alkoxide ion is oxidized to a ketone, while the anionic charge is shifted to the O1 atom. The change of the magnesium positions along the hydride transfer reaction coordinate has been recorded from combined QM/MM molecular dynamics simulations and the study of XyI's kinetic isotope effects (Figure 7). Positions 1 and 2 of Mg2 in the X-ray structure with glucose substrate encompass the entire range of the average Mg–Mg distances along the hydride transfer reaction coordinate,[147] and the average Mg1–Mg2 distance at the hydride transfer transition state has a value that is very similar to the distance (4.2 Å) found in the X-ray structure for a TS analogue inhibitor.[156] These findings provide a dynamical demonstration of the postulated role of these two metal sites in catalysis; they modulate the charge migrations for the entire XyI reaction process through cofactor breathing motions.[150,151] This metal breathing motion, in the ligand-bridged bimetallic motif, provides the dominant force that promotes the hydride shift from C2 to C1.

Dihydrofolate reductase (DHFR) catalyzes the formal hydrogenation of 7,8-dihydrofolate to tetrahydrofolate with the rate-limiting step being the hydride transfer step from the cofactor nicotinamide adenine dinucleotide phosphate (NADPH). An intriguing experimental finding was that amino acid mutations that are far away from the active site can have large effects, in particular reducing the $k_{cat}$ value.[254] Since these residues do not directly participate in hydrogen bonding interactions with the substrate, the enzyme kinetics must be affected either by a change in enzyme dynamics or by a change in structural features that propagate to the active site through hydrogen bonding networks. The mechanism and kinetic isotope effects have been investigated extensively.[34,73,122,254–270] Here, we highlight the observation of structural changes along the reaction pathway, especially the change in hydrogen bond distance that leads to transition state stabilization. DHFR is a rather small protein but binds to a large cofactor and a large substrate. This may be one reason protein

flexibility is especially important for substrate binding, product release, and protection of the active site. Indeed, a flexible loop has been observed in X-ray structures to occupy at least three different conformations, in the presence and absence of substrate and transition state analogue inhibitors.[39] Early molecular dynamics simulations characterized conformational differences corresponding to various stages of the hydride transfer reaction, both for the wild-type and for mutant enzymes,[271,272] suggesting that structural correlations can be global and involved in the catalytic process, which are in accord with NMR experiments.[273,274] Brooks and co-workers studied this by carrying out minimum-energy-path calculations starting from configurations from a long-time molecular dynamics trajectory; from the statistical distribution of reaction paths and protein conformations for the wild-type, Gly121Ser, and Gly121Val mutant, they found that certain distinct protein conformational substates provide environments that modify the reaction barrier, and these conformational substates can be correlated to the observed rate constants.[268,269] More recently, these analyses have been extended to PMF calculations, also showing the significant role of distant mutations in altering protein conformational substates.[270]

Hammes-Schiffer and co-workers examined the variations of a series of hydrogen bond distances as a function of a collective solvent reaction coordinate for the hydride transfer, and these changes in modes other than the reaction coordinate have been called coupled promoting motions. They do not necessarily occur on the same time scale as hydride transfer or concomitantly with it in real time, but rather represent statistical mechanical correlations in the equilibrium thermodynamic ensemble.[33,73] It was found that some of the hydrogen bonding interactions were interrupted in the Gly121Val mutant, which has been attributed to increasing the hydride transfer barrier.[172,275] The change of hydrogen bonding network along the hydride transfer reaction pathway has been analyzed over QM/MM dynamic trajectories mapped along the reaction coordinate by Garcia-Viloca et al.,[122] and similar observations were obtained as in the work of Agarwal et al., who used different force fields and a different reaction coordinate. The qualitative interpretation of the change of these hydrogen bonds on transition state stabilization was confirmed by evaluation of specific interaction energies. It was found that hydrogen bonding interactions that stabilize the transition state also stabilize the product state. More importantly, a number of hydrogen bonds that do not show significant change during the hydride transfer reaction contribute large transition state stabilization, suggesting that structural analyses should be coupled to energy calculations.[122] It was also found that the electronic polarization is more pronounced with greater stabilizations at the transition state than in the reactant state.[94,276]

Correlation of catalysis with the change in average hydrogen bond distance in the enzyme has been analyzed for other systems, including the PTP phosphate hydrolysis reaction, and its origin in that case was attributed to the Walden inversion mechanism in the nucleophilic substitution reaction.[193,194]

## 3.4. Quantum Mechanical Effects

The significance of quantum mechanical tunneling effects in enzymatic reactions was appreciated through the pioneering work of Klinman, Schowen, and others.[277–280] This topic is discussed in great detail in this issue; hence, readers are directed to the

accompanying paper in this issue for further discussion.[34] However, it is important to emphasize here that although computational and experimental studies indicate that quantum mechanical tunneling makes only relatively small contributions to the reduction of the free energy barrier for the enzymatic reaction relative to that of the uncatalyzed reaction in water, it is still essential to include quantum mechanical effects, which include both zero-point energies and tunneling, to determine the absolute rate constant. Moreover, from a fundamental point of view, since proton, hydride, and hydrogen atom transfer reactions are dominated by tunneling events, any description purely in terms of classical mechanics is not satisfying. Inclusion of zero-point motion means that the high-frequency modes explore a wider region of the potential energy surface with appreciable probability than is traversed by classical trajectories in a canonical ensemble. Furthermore, computed kinetic isotope effects are in agreement with experiments only when quantized vibrations and tunneling are included in the computational procedure. In Table 2, we summarize some of the computed KIEs for several enzymes, along with the experimental data. We point out that the proton abstraction reaction by methylamine dehydrogenase has remarkably large primary isotope effects, and the overall quantum effects lower the free energy of activation by 5.7 kcal/mol in comparison with that obtained without including these contributions.[281] Of the total quantum effects on this reaction rate, 2.5 kcal/mol are due to zero-point energy difference, while tunneling contributes 3.2 kcal/mol.

## 3.5. Balancing Kinetics and Thermodynamics

The remarkable ability that enzymes have to control chemical reactivity is demonstrated by the regio- and stereoselectivity in the enzymatic cyclization of squalene and 2,3-oxidosqualene to form polycyclic triterpenes.[282] The former reaction yields the hopene skeleton, a precursor that condenses bacterial membranes.[283] The latter eukaryotic process leads to lanosterol, which is further converted to cholesterol.[284–286] Recently, the crystal structures of several terpenoid cyclases have been determined, providing an opportunity to examine the mechanism of these enzymatic processes that in many cases produce the disfavored anti-Markovnikov carbocation intermediate in the cyclization cascade.

To this end, the carbocation cyclization reaction by squalene to hopene cyclase (SHC) has been studied using a combined QM(AM1)/MM potential through molecular dynamics simulations. By dissecting the overall reaction, which consists of the formation of five rings and nine stereocenters, into several steps that can be modeled computationally, Rajamani and Gao constructed several two-dimensional free energy reaction profiles to address the questions of concerted versus stepwise processes and the selectivity of Markovnikov and anti-Markovnikov pathways.[22] The final free energy results for the overall carbocation cyclization cascade are summarized in Figure 8, which shows the free energy barriers and the free energies of reaction for the formation of various stable carbenium ion intermediates in SHC. The reaction coordinate in this diagram is a representation of the minimum free energy paths from several two-dimensional free energy contours. Based on this free energy profile, a revised reaction pathway has been proposed, which is duplicated in Scheme 4.

A key finding is a delicate balance of thermodynamic and kinetic control in the squalene-to-hopene cation cyclization. To avoid the tricyclic cyclopentylcarbinyl cation, **IV**, which

would be a favored Markovnikov product, the enzyme raises its free energy so that a rapid equilibrium can be established with **III** with little reaction barrier. Consequently, its lifetime is expected to be similar to that of **III**, and elimination and addition reactions with the solvent do not occur, and thus the enzyme does not need to avoid its formation because it will not proceed further. The completion of the cyclization steps is highly favored thermodynamically, but the enzyme controls the formation of the major product **VIII** (99%) by a faster reaction rate (lower reaction barrier) than the formation of the side product **VI** (1%).[22] The overall cyclization process releases nearly 60 kcal/mol of energy.

In another study of the sesquiterpene cyclase, trichodiene cyclase, which converts farnesyl diphosphate into trichodiene, a precursor carbon skeleton for numerous antibiotics and for fusion of cell walls, was modeled by combined QM/MM free energy simulations.[287] In this reaction, the formation of the five-membered ring via an anti-Markovnikov cyclopentylcarbinyl cation is thermodynamically competitive to the formation of the Markovnikov intermediate in a four-membered ring system. The initial cationic intermediate is not produced in the most favorable binding pocket. The overall cyclization reaction is controlled by the subsequent hydride transfer step, which is rate limiting. These findings agree with experiments. On the basis of X-ray structures that include reactant and transition state analogue inhibitors plus the pyrophosphate species, coupled with biochemical and mutational studies, Cane and co-workers proposed that the trichodiene cyclization reaction is controlled kinetically, avoiding the most favorable cation–anion interactions that would lead to premature termination and side products.[23,42]

## 4. Conclusions

In this review, we summarize the theory and computational techniques for studying enzymatic reactions. We highlight the identification of key features that lower the free energy of activation relative to the uncatalyzed reaction in water.

We emphasize the need for validating potential energy functions, whether they are based on quantum mechanical models or are purely empirical functions, by comparison with both structural and energetic results for the reaction in the gas phase and for bimolecular hydrogen bonding complexes, with data on the latter taken from experiments or high-level ab initio calculations. In comparison, parametrizing potential functions to reproduce experimental data in water is less reliable because there can be cancellation of errors in intrinsic substrate properties and solvation effects.

We emphasize that to understand the factors that contribute to catalysis, it is important to determine solvation effects by free energy simulations. For this purpose, we discuss how solvent effects and enzymatic catalysis are studied by carrying out umbrella sampling free energy simulations to obtain the potentials of mean force for the uncatalyzed and catalyzed reactions. We point out that the difference in free energy of activation determined from potential of mean force calculations does not necessarily equal the solvation free energy difference for the reactant and transition state from free energy perturbation theory, unless there is only small change in protein conformation during the enzymatic reaction.

Examining a variety of enzymatic reactions that are well-understood from experiments and computations, we found that natural selection enables enzymes to achieve catalytic efficiency in many different ways. The factors promoting catalysis include transition state stabilization through electrostatic interactions, desolvation and reactant state destabilization, protein conformational change induced by differential interactions between the substrate and enzyme in the reactant state and transition state, and general acid and general base catalysis. Quantum mechanical tunneling is also critical in some enzyme reactions especially if the absolute rate constants and kinetic isotope effects are to be understood and properly interpreted. In some systems such as the terpenoid cyclization reactions, enzymes employ a delicate balance of kinetic and thermodynamic control to determine the regio- and stereoselectivity and protect the highly reactive carbocation intermediates from side reactions.

## Acknowledgments

## Biographies



Jiali Gao received a B.S. in Chemistry from Beijing University in 1982. He came to Purdue University through a Graduate Program of 43 students, arranged by William von E. Doering, and obtained a Ph.D. in 1987 under the guidance of William L. Jorgensen. The original intention of the program was that these students would return to China after graduate studies in America; however, events taking place in 1989 made it impossible. He became a naturalized citizen of the United States in 1998, and he has since rigorously performed his duties as a citizen. After postdoctoral research with Martin Karplus at Harvard, the State University of New York at Buffalo offered him an opportunity to pursue his independent research and teaching in 1990. Since 2000, he has been on the faculty of the University of Minnesota, where he is Professor of Chemistry. His research interests include computational studies of chemical and biological problems. He is a recipient of the 2000 Dirac Medal from the World Association for Theoretically Oriented Chemists.



Shuhua Ma received a B.S. degree in Chemistry in 1995 from Beijing Normal University, P. R. China. She continued studying in Beijing Normal University until 1998, when she got a

M.S. degree in Physical Chemistry-Electrochemistry with Professor Zhongda Wu and Professor Zhenghao Wang. She then moved to Institute of Chemistry, Chinese Academy of Sciences, and received her Ph.D. degree in Physical Chemistry-Quantum Chemistry in 2001; her advisors were Professor Qiyuan Zhang and Professor Zhongheng Yu. She is a postdoctoral associate in the research group of Dr. Jiali Gao at Department of Chemistry, University of Minnesota. Her current research focuses on molecular simulation of enzyme catalysis, protein–DNA interactions, and computer-aided drug design.



Dan Major was born in Norway in 1973. He received his B.Sc. (magna cum laude) in chemistry and computer science and Ph.D. in computational chemistry from Bar-Ilan University in Israel. He is a Fulbright scholar currently on a postdoctoral stay with Prof. Jiali Gao at the University of Minnesota. His research interests include theoretical study of chemical and enzymatic reactions and molecular recognition in receptors.
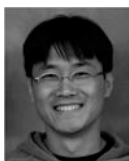


Kwangho Nam was born in Korea (1972) and received a B.A. (1995) and a M.A. (1998) in agricultural chemistry from Korea University, Seoul, Korea. After finishing a military service, he came to the University of Minnesota in 2001 to pursue a Ph.D. in chemistry and is currently working jointly for Jiali Gao and Darrin M. York. His research interests include the study of chemical reactions in biophysical systems using various computational methods and the design of new theoretical methods with focus on the combined QM/MM methods to model the reactions in the condensed phase.



Jingzhi Pu was born in Beijing, China, in 1976. He received a B.A. in Chemistry from Peking University in 1999 and a Ph.D. from the University of Minnesota in 2004 under the direction of Donald G. Truhlar. After finishing a short postdoctoral study with Jiali Gao, he moved to Boston. He is currently a postdoctoral associate at Harvard with Martin Karplus. His recent research interests include quantum effects in enzymatic reactions and protein dynamics. He has been married to Yan He since 2002.

Donald G. Truhlar was born in Chicago in 1944. He received a B.A. in Chemistry from St. Mary's College of Minnesota in 1965 and a Ph.D. from Caltech in 1970 under the direction of Aron Kuppermannn. He has been on the faculty of the University of Minnesota since 1969, where he is currently Lloyd H. Reyerson Professor of Chemistry, Chemical Physics, Scientific Computation, and Nanoparticle Science and Engineering. His research interests are theoretical and computational chemical dynamics and molecular structure and energetics. He is the author of over 800 scientific publications, and he has received several awards for his research, including a Sloan Fellowship, Fellowships in the American Physical Society and the American Association for the Advancement of Science, an NSF Creativity Award, the ACS Award for Computers in Chemical and Pharmaceutical Research, the Minnesota Award, the National Academy of Sciences Award for Scientific Reviewing, the ACS Peter Debye Award for Physical Chemistry, and the Schrödinger Medal of The World Association of Theoretical and Computational Chemists. He has been married to Jane Truhlar since 1965, and he has two children, Sara Elizabeth Truhlar and Stephanie Marie Eaton Truhlar.

## References

1. Schowen, RL. Transition States of Biochemical Processes. Gandour, RD.; Schowen, RL., editors. New York: Plenum Press; 1978. p. 77

2. Wolfenden R, Snider MJ. Acc. Chem. Res. 2001; 34:938. [PubMed: 11747411]

3. Lad C, Williams NH, Wolfenden R. Proc. Natl. Acad. Sci. U.S.A. 2003; 100:5607. [PubMed: 12721374]

4. Knowles JR, Albery WJ. Acc. Chem. Res. 1977; 10:105.

5. Radzicka A, Wolfenden R. Science. 1995; 267:90. [PubMed: 7809611]

6. Wu N, Mo Y, Gao J, Pai EF. Proc. Natl. Acad. Sci. U.S.A. 2000; 97:2017. [PubMed: 10681441]

7. Garcia-Viloca M, Gao J, Karplus M, Truhlar DG. Science. 2004; 303:186. [PubMed: 14716003]

8. Snider MG, Temple BS, Wolfenden R. J. Phys. Org. Chem. 2004; 17:586.

9. Walsh, C. Enzymatic Reaction Mechanisms. San Francisco, CA: Freeman; 1979.

10. Warshel A. Annu. Rev. Biophys. Biomol. Struct. 2003; 32:425. [PubMed: 12574064]

11. Gao J. Acc. Chem. Res. 1996; 29:298.

12. Gao J, Truhlar DG. Annu. Rev. Phys. Chem. 2002; 53:467. [PubMed: 11972016]

13. Truhlar DG, Gao J, Alhambra C, Garcia-Viloca M, Corchado J, Sanchez ML, Villa J. Acc. Chem. Res. 2002; 35:341. [PubMed: 12069618]

14. Merz KM Jr. ACS Symp. Ser. 1998; 712:2.

15. Antes I, Thiel W. ACS Symp. Ser. 1998; 712:50.

16. Assfeld X, Ferre N, Rivail J-L. ACS Symp. Ser. 1998; 712:234.

17. Cummins PL, Gready JE. ACS Symp. Ser. 1998; 712:250.

18. Moliner V, Andres J, Oliva M, Safont VS, Tapia O. Theor. Chem. Acc. 1999; 101:228.

19. Tresadern G, Nunez S, Faulder PF, Wang H, Hillier IH, Burton NA. Faraday Discuss. 2002; 122:223. [PubMed: 12555860]

20. Cui Q, Karplus M. Adv. Prot. Chem. 2003; 66:315.

21. Cane, DE., editor. Comprehensive Natural Product Chemistry: Isoprenoids including Carotenoids, and Steroids. Vol. 2. Oxford, U.K.: Elsevier; 1999.

22. Rajamani R, Gao J. J. Am. Chem. Soc. 2003; 125:12768. [PubMed: 14558824]

23. Vedula LS, Cane DE, Christianson DW. Biochemistry. 2005; 44:12719. [PubMed: 16171386]

24. Eyring H, Stearn AE. Chem. Rev. 1939; 24:253.

25. Glasstone, S.; Laidler, KJ.; Eyring, H. The Theory of Rate Processes. New York: McGraw-Hill; 1941.

26. Truhlar, DG.; Hase, WL.; Hynes, JT. J. Phys. Chem. Vol. 87. Erratum; 1983. **1983**, 87, 5523.

27. Wynne-Jones WFK, Eyring H. J. Chem. Phys. 1935; 3:492.Evans MG. Trans. Faraday Soc. 1938; 34:49.

28. Hill, TL. An Introduction to Statistical Thermodynamics. Reading, MA: Addison-Wesley; 1960.

29. Schenter GK, Garrett BC, Truhlar DG. J. Chem. Phys. 2003; 119:5828.

30. Torrie GM, Valleau JP. J. Comput. Phys. 1977; 23:187.

31. Voth GA, Hochstrasser RM. J. Phys. Chem. 1996; 100:13034.

32. Villa J, Warshel A. J. Phys. Chem. B. 2001; 105:7887.

33. Benkovic SJ, Hammes-Schiffer S. Science. 2003; 301:1196. [PubMed: 12947189]

34. Pu J, Gao J, Truhlar DG. Chem. Rev. 2006; 106:3140–3169. http://dx.doi.org/10.1021/cr050308e. [PubMed: 16895322]

35. Fersht, A. Structure and Mechanism in Protein Science. New York: W. H. Freeman and Company; 1998.

36. Bruice TC, Benkovic SJ. Biochemistry. 2000; 39:6267. [PubMed: 10828939]

37. Zhang X, Houk KN. Acc. Chem. Res. 2005; 38:379. [PubMed: 15895975]

38. Gandour, RD.; Schowen, RL., editors. Transition States of Biochemical Processes. New York: Plenum Press; 1978.

39. Sawaya MR, Kraut J. Biochemistry. 36:586. [PubMed: 9012674]

40. Davenport RC, Bash PA, Seaton BA, Karplus M, Petsko GA, Ringe D. Biochemistry. 1991; 30:5821. [PubMed: 2043623]

41. Jogl G, Rozovsky S, McDermott A, Tong L. Proc. Natl. Acad. Sci. U.S.A. 2003; 100:50. [PubMed: 12509510]

42. Vedula LS, Rynkiewicz MJ, Pyun H-J, Coates RM, Cane DE, Christianson DW. Biochemistry. 2005; 44:6153. [PubMed: 15835903]

43. Gao J. Curr. Opin. Struct. Biol. 2003; 13:184. [PubMed: 12727511]

44. Gao J, Byun KL, Kluger R. Top. Curr. Chem. 2004; 238:113.

45. Kollman P. Chem. Rev. 1993; 93:2395.

46. Warshel A, Strajbl M, Villa J, Florian J. Biochemistry. 2000; 39:14728. [PubMed: 11101287]

47. Olsson MHM, Warshel A. J. Am. Chem. Soc. 2004; 126:15167. [PubMed: 15548014]

48. Gao J, Furlani TR. IEEE Comput. Sci. Eng. 1995 Fall;(Issue):24.

49. Atkins, P.; Friedman, R. Molecular Quantum Mechanics. 4th ed.. New York: Oxford University Press; 2000. p. 249ff.

50. MacKerell AD Jr, Bashford D, Bellott M, Dunbrack RL, Evanseck JD, Field MJ, Fischer S, Gao J, Guo H, Ha S, Joseph-McCarthy D, Kuchnir L, Kuczera K, Lau FTK, Mattos C, Michnick S, Ngo T, Nguyen DT, Prodhom B, Reiher WE III, Roux B, Schlenkrich M, Smith JC, Stote R, Straub J, Watanabe M, Wiorkiewicz-Kuczera J, Yin D, Karplus M. J. Phys. Chem. B. 1998; 102:3586. [PubMed: 24889800]

51. van Gunsteren, WF.; Berendsen, HJC. Biomass. Groningen; 1987.

52. MacKerell, AD, Jr. Computational Biochemistry and Biophysics. Becker, OM.; MacKerell, AD., Jr; Roux, B.; Watanabe, M., editors. New York: Dekker; 2001. p. 7

53. Cramer, CJ. Essentials of Computational Chemistry. 2nd ed.. Chichester, U.K.: John Wiley & Sons; 2004.

54. Ponder JW, Case DA. Adv. Protein Chem. 2003; 66:27. [PubMed: 14631816]

55. Chandrasekhar J, Smith SF, Jorgensen WL. J. Am. Chem. Soc. 1984; 106:3049.

56. Chandrasekhar J, Smith SF, Jorgensen WL. J. Am. Chem. Soc. 1985; 107:154.

57. Donini O, Darden T, Kollman PA. J. Am. Chem. Soc. 2000; 122:12270.

58. Zhang YK, Liu HY, Yang WT. J. Chem. Phys. 2000; 112:3483.

59. Liu H, Lu Z, Cisneros GA, Yang W. J. Chem. Phys. 2004; 121:697. [PubMed: 15260596]

60. Warshel, A. Computer Modeling of Chemical Reactions in Enzymes and Solutions. New York: Wiley; 1991.

61. Warshel A, Weiss RM. J. Am. Chem. Soc. 1980; 102:6218.

62. London F. Z. Elektrochem. 1929; 35:551.

63. Eyring H, Polanyi M. Naturwissenschaften. 1930; 18:914.

64. Sato S. Bull. Chem. Soc. Jpn. 1955; 28:450.

65. Tully JC. Mod. Theor. Chem. 1977; 7:173.

66. Kim Y, Corchado JC, Villa J, Xing J, Truhlar DG. J. Chem. Phys. 2000; 112:2718.

67. Aaqvist J, Warshel A. Chem. Rev. 1993; 93:2523.

68. Mo Y, Gao J. J. Phys. Chem. A. 2000; 104:3012.

69. Gao, J.; Mo, Y. Theoretical Methods in Condensed Phase Chemistry. Schwartz, SD., editor. Dordrecht, The Netherlands: Kluwer Academic Publishers; 2000. p. 247

70. Gao J, Garcia-Viloca M, Poulsen TD, Mo Y. Adv. Phys. Org. Chem. 2003; 38:161.

71. Neria E, Karplus M. Chem. Phys. Lett. 1997; 267:26.

72. Schmitt UW, Voth GA. J. Phys. Chem. B. 1998; 102:5547.

73. Agarwal PK, Billeter SR, Rajagopalan PTR, Benkovic SJ, Hammes-Schiffer S. Proc. Natl. Acad. Sci. 2002; 99:2794. [PubMed: 11867722]

74. Boggs JE. J. Comput. Chem. 1999; 20:1587.

75. Liu H, Elstner M, Kaxiras E, Fraunheim T, Hermans J, Yang W. Proteins: Struct., Funct., Genet. 2001; 44:484. [PubMed: 11484226]

76. Monard G, Merz KM Jr. Acc. Chem. Res. 1999; 32:904.

77. Car R, Parrinello M. Phys. Rev. Lett. 1985; 55:2471. [PubMed: 10032153]

78. Tuckerman ME, Laasonen K, Sprik M, Parrinello M. J. Phys.: Condens. Matter. 1994; 6:A93.

79. Sprik M, Hutter J, Parrinello M. J. Chem. Phys. 1996; 105:1142.

80. Rothlisberger U, Carloni P, Doclo K, Parrinello M. J. Biol. Inorg. Chem. 2000; 5:236. [PubMed: 10819469]

81. Kuo IFW, Mundy CJ, McGrath MJ, Siepmann JI, VandeVondele J, Sprik M, Hutter J, Chen B, Klein ML, Mohamed F, Krack M, Parrinello M. J. Phys. Chem. B. 2004; 108:12990.

82. Rovira C. Chem Phys Chem. 2005; 6:1685.

83. Rohrig UF, Guidoni L, Rothlisberger U. Chem Phys Chem. 2005; 6:1836. [PubMed: 16110519]

84. York DM, Lee T-S, Yang W. Phys. Rev. Lett. 1998; 80:5011.

85. Titmuss SJ, Cummins PL, Rendell AP, Bliznyuk AA, Gready JE. J. Comput. Chem. 2002; 23:1314. [PubMed: 12214314]

86. Van der Vaart A, Merz KM Jr. J. Am. Chem. Soc. 1999; 121:9182.

87. Stewart JJP. Int J. Quantum Chem. 1996; 58:133.

88. Warshel A, Levitt M. J. Mol. Biol. 1976; 103:227. [PubMed: 985660]

89. Singh UC, Kollman PA. J. Comput. Chem. 1986; 7:718.

90. Field MJ, Bash PA, Karplus M. J. Comput. Chem. 1990; 11:700.

91. Waszkowycz B, Hillier IH, Gensmantel N, Payling DW. J. Chem. Soc., Perkin Trans. 1991; 2:225.

92. Gao, J. Reviews in Computational Chemistry. Lipkowitz, KB.; Boyd, DB., editors. Vol. 7. New York: VCH; 1995. p. 119

93. Gao J, Xia X. Science. 1992; 258:631. [PubMed: 1411573]

94. Garcia-Viloca M, Truhlar DG, Gao J. J. Mol. Biol. 2003; 327:549. [PubMed: 12628257]

95. Hillier IH. THEOCHEM. 1999; 463:45.Mulholland AJ. Theor. Comput. Chem. 2001; 9:597.

96. Morokuma K. Philos. Trans. R. Soc. London, Ser. A. 2002; 360:1149.

97. Lin H, Truhlar DG. Theor. Chem. Acc. in press.

98. Sherwood, P. Modern Methods and Algorithms of Quantum Chemistry. Grotendorst, J., editor. Vol. 3. Princeton, NJ: NIC-Directors; 2000. p. 285

99. Dewar MJS, Thiel W. J Am. Chem. Soc. 1977; 99:4899.

100. Dewar MJS, Zoebisch EG, Healy EF, Stewart JJP. J. Am. Chem. Soc. 1985; 107:3902.

101. Stewart JJP. J. Comput. Chem. 1989; 10:209.

102. Hehre, WJ.; Radom, L.; Schleyer, PvR; Pople, JA. Ab Initio Molecular Orbital Theory. New York: John Wiley & Sons; 1986.

103. Parr, RG.; Yang, W. Density Functional Theory of Atoms and Molecules. London: Oxford University Press; 1989.

104. Stephens PJ, Devlin FJ, Chabalowski CF, Frisch MJ. J. Phys. Chem. 1994; 98:11623.

105. Becke AD. Phys. Rev. A. 1988; 38:3098. [PubMed: 9900728]

106. Lee C, Yang W, Parr RG. Phys. Rev. B. 1988; 37:785.

107. Adamo C, Barone V. J. Chem. Phys. 1997; 104:1040.

108. Zhao Y, Truhlar DG. J. Phys. Chem. A. 2005; 109:5656. [PubMed: 16833898]

109. Zhao Y, Schultz NE, Truhlar DG. J. Chem. Theory Comput. 2006; 2:364.

110. Gelin BR, Karplus M. Proc. Natl. Acad. Sci. U.S.A. 1975; 72:2002. [PubMed: 1056008]

111. Meuwly M, Becker OM, Stote R, Karplus M. Biophys. Chem. 2002; 98:183. [PubMed: 12128198]

112. Zhang X, Bruice TC. Proc. Natl. Acad. Sci. U.S.A. 2005; 102:18356. [PubMed: 16344484]

113. Hur S, Bruice TC. J. Am. Chem. Soc. 2003; 125:5964. [PubMed: 12733937]

114. Gonzalez-Lafont A, Truong TN, Truhlar DG. J. Phys. Chem. 1991; 95:4618.

115. Alhambra C, Luz Sanchez M, Corchado J, Gao J, Truhlar DG. Chem. Phys. Lett. 2001; 347:512.

116. Lau EY, Kahn K, Bash PA, Bruice TC. Proc. Natl. Acad. Sci. U.S.A. 2000; 97:9937. [PubMed: 10963662]

117. Ferrer S, Ruiz-Pernia JJ, Tunon I, Moliner V, Garcia-Viloca M, Gonzalez-Lafont A, Lluch JM. J. Chem. Theory Comput. 2005; 1:750.

118. Cui Q, Karplus M. J. Phys. Chem. B. 2002; 106:1768.

119. Ridder L, Rietjens IMCM, Vervoort J, Mulholland AJ. J. Am. Chem. Soc. 2002; 124:9926. [PubMed: 12175255]

120. Alhambra C, Gao J, Corchado JC, Villa J, Truhlar DG. J. Am. Chem. Soc. 1999; 121:2253.

121. Devi-Kesavan Lakshmi S, Garcia-Viloca M, Gao J. Theor. Chem. Acc. 2003; 109:133.

122. Garcia-Viloca M, Truhlar DG, Gao J. Biochemistry. 2003; 42:13558. [PubMed: 14622003]

123. Tubert-Brohman I, Guimaraes CRW, Repasky MP, Jorgensen WL. J. Comput. Chem. 2003; 25:138. [PubMed: 14635001]

124. Tubert-Brohman I, Guimaraes CRW, Jorgensen WL. J. Chem. Theory Comput. 2005; 1:817. [PubMed: 19011692]

125. Guimaraes CRW, Udier-Blagovic M, Tubert-Brohman I, Jorgensen WL. J. Chem. Theory Comput. 2005; 1:617.

126. Guimaraes CRW, Udier-Blagovic M, Jorgensen WL. J. Am. Chem. Soc. 2005; 127:3577. [PubMed: 15755179]

127. Gao J. Proc. Ind. Acad. Sci. 1994; 106:507.

128. Byun K, Mo Y, Gao J. J. Am. Chem. Soc. 2001; 123:3974. [PubMed: 11457147]

129. Corchado JC, Espinosa-Garcia J, Hu W-P, Rossi I, Truhlar DG. J. Phys. Chem. 1995; 99:687.

130. Corchado JC, Truhlar DG. ACS Symp. Ser. 1998; 712:106.

131. Gao J. J. Chem. Phys. 1998; 109:2346.

132. Freindorf M, Gao J. J. Comput. Chem. 1996; 17:386.

133. Riccardi D, Li G, Cui Q. J. Phys. Chem. B. 2004; 108:6467. [PubMed: 18950136]

134. Maseras F, Morokuma K. J. Comput. Chem. 1995; 16:1170.

135. Matsubara T, Maseras F, Koga N, Morokuma K. J. Phys. Chem. 1996; 100:2573.

136. Marti S, Moliner V, Tunon I. J. Chem. Theory Comput. 2005; 1:1008.

137. Thomas A, Field MJ. J. Am. Chem. Soc. 2002; 124:12432. [PubMed: 12381183]

138. Poulsen TD, Garcia-Viloca M, Gao J, Truhlar DG. J. Phys. Chem. B. 2003; 107:9567.

139. Gao J. ACS Symp. Ser. 1994; 569:8.

140. Valleau, JP.; Torrie, GM. Modern Theoretical Chemistry. Berne, BJ., editor. Vol. 5. New York: Plenum; 1977. p. 169

141. Zwanzig R. J. Chem. Phys. 1954; 22:1420.

142. Jorgensen WL, Ravimohan C. J. Chem. Phys. 1985; 83:3050.

143. Simonson, T. Computational Biochemistry and Biophysics. Becker, OM.; MacKerell, AD., Jr; Roux, B.; Watanabe, M., editors. New York: Dekker; 2001. p. 169

144. Kollman PA, Kuhn B, Donini O, Perakyla M, Stanton R, Bakowies D. Acc. Chem. Res. 2001; 34:72. [PubMed: 11170358]

145. Koshland DE Jr. Adv. Enzymol. 1960; 22:45.

146. Lu N, Wu D, Woolf TB, Kofke DA. Phys. Rev. E: Stat., Nonlin., Soft Matter Phys. 2004; 69 No. 057702/057701.

147. Lavie A, Allen KN, Petsko GA, Ringe D. Biochemistry. 1994; 33:5469. [PubMed: 8180169]

148. Garcia-Viloca M, Poulsen TD, Truhlar DG, Gao J. Protein Sci. 2004; 13:2341. [PubMed: 15322278]

149. Bhattacharyya S, Ma S, Stankovich MT, Truhlar DG, Gao J. Biochemistry. 2005; 44:16549. [PubMed: 16342946]

150. Garcia-Viloca M, Alhambra C, Truhlar DG, Gao. J. Am. Chem. Soc. 2002; 124:7268. [PubMed: 12071725]

151. Garcia-Viloca M, Alhambra C, Truhlar DG, Gao J. J. Comput. Chem. 2003; 24:177. [PubMed: 12497598]

152. Ghisla S, Thorpe C. Eur. J. Biochem. 2004; 271:494. [PubMed: 14728676]

153. Djordjevic S, Pace CP, Stankovich MT, Kim J-JP. Biochemistry. 1995; 34:2163. [PubMed: 7857927]

154. Satoh A, Nakajima Y, Miyahara I, Hirotsu K, Tanaka T, Nishina Y, Shiga K, Tamaoki H, Setoyama C, Miura R. J. Biochem. 2003; 134:297. [PubMed: 12966080]

155. Allen KN, Lavie A, Glasfeld A, Tanada TN, Gerrity DP, Carlson SC, Farber GK, Petsko GA, Ringe D. Biochemistry. 1994; 33:1488. [PubMed: 7906142]

156. Allen KN, Lavie A, Petsko GA, Ringe D. Biochemistry. 1995; 34:3742. [PubMed: 7893671]

157. Carrell HL, Glusker JP, Burger V, Manfre F, Tritsch D, Biellmann JF. Proc. Natl. Acad. Sci. U.S.A. 1989; 86:4440. [PubMed: 2734296]

158. Farber GK, Machin P, Almo SC, Petsko GA, Hajdu J. Proc. Natl. Acad. Sci. U.S.A. 1988; 85:112. [PubMed: 3422408]

159. Whitlow M, Howard AJ, Finzel BC, Poulos Thomas L, Winborne E, Gilliland GL. Proteins: Struct., Funct., Genet. 1991; 9:153. [PubMed: 2006134]

160. Amyes TL, Richard JP, Tait JJ. J. Am. Chem. Soc. 2005; 127:15708. [PubMed: 16277505]

161. Wu N, Pai EF. J. Biol. Chem. 2002; 277:28080. [PubMed: 12011084]

162. Wu N, Gillon W, Pai EF. Biochemistry. 2002; 41:4002. [PubMed: 11900543]

163. Wu N, Pai EF. Top. Curr. Chem. 2004; 238:23.

164. Begley TP, Appleby TC, Ealick SE. Curr. Opin. Struct. Biol. 2000; 10:711. [PubMed: 11114509]

165. Appleby TC, Kinsland C, Begley TP, Ealick SE. Proc. Natl. Acad. Sci. U.S.A. 2000; 97:2005. [PubMed: 10681442]

166. Raugei S, Cascella M, Carloni P. J. Am. Chem. Soc. 2004; 126:15730. [PubMed: 15571395]

167. Cui Q, Karplus M. J. Phys. Chem. B. 2002; 106:7927.

168. Wang M, Lu Z, Yang W. J. Chem. Phys. 2004; 121:101. [PubMed: 15260526]

169. Nam K, Prat-Resina X, Garcia-Viloca M, Devi-Kesavan LS, Gao J. J. Am. Chem. Soc. 2004; 126:1369. [PubMed: 14759194]

170. Soriano A, Silla E, Tunon I, Ruiz-Lopez MF. J. Am. Chem. Soc. 2005; 127:1946. [PubMed: 15701029]

171. Warshel A, Chu ZT, Parson WW. Science. 1989; 246:112. [PubMed: 2675313]

172. Watney JB, Agarwal PK, Hammes-Schiffer S. J. Am. Chem. Soc. 2003; 125:3745. [PubMed: 12656604]

173. Elber R, Karplus M. Chem. Phys. Lett. 1987; 139:375.

174. Elber R, Karplus M. J. Am. Chem. Soc. 1990; 112:9161.

175. Elber R. J. Chem. Phys. 1990; 93:4312.

176. Dellago C, Bolhuis PG, Chandler D. J. Chem. Phys. 1998; 108:9236.

177. Dellago C, Bolhuis PG, Csajka FS, Chandler D. J. Chem. Phys. 1998; 108:1964.

178. Dellago C, Bolhuis PG, Chandler D. J. Chem. Phys. 1999; 110:6617.

179. Voter AF. J. Chem. Phys. 1997; 78:3908.

180. Henkelman G, Uberuaga BP, Jonsson H. J. Chem. Phys. 2000; 113:9901.

181. Gonzalez-Garcia N, Pu J, Gozalez-Lafont A, Lluch JM, Truhlar DG. J. Chem. Theory Comput. 2006; 2 http://dx.doi.org/10.1021/ct060032y.

182. Muller RP, Warshel A. J. Phys. Chem. 1995; 99:17516.

183. Schenter GK, Garrett BC, Truhlar DG. J. Phys. Chem. B. 2001; 105:9672.

184. Gerlt JA, Gassman PG. J. Am. Chem. Soc. 1992; 114:5928.

185. Wedekind JE, Reed GH, Rayment I. Biochemistry. 1995; 34:4325. [PubMed: 7703246]

186. Larsen TM, Wedekind JE, Rayment I, Reed GH. Biochemistry. 1996; 35:4349. [PubMed: 8605183]

187. Liu H, Zhang Y, Yang W. J. Am. Chem. Soc. 2000; 122:6560.

188. Poyner RR, Laughlin LT, Sowa GA, Reed GH. Biochemistry. 1996; 35:1692. [PubMed: 8634301]

189. Zhang ZY, Wang Y, Dixon JE. Proc. Natl. Acad. Sci. U.S.A. 1994; 91:1624. [PubMed: 8127855]

190. Zhang Z, Harms E, Van Etten RL. J. Biol. Chem. 1994; 269:25947. [PubMed: 7929301]

191. Barford D, Flint AJ, Tonks NK. Science. 1994; 263:1397. [PubMed: 8128219]

192. Zhang Z-Y. Curr. Top. Cell. Regul. 1997; 35:21. [PubMed: 9192175]

193. Alhambra C, Wu L, Zhang Z-Y, Gao J. J. Am. Chem. Soc. 1998; 120:3858.

194. Alhambra C, Gao J. J. Comput. Chem. 2000; 21:1192.

195. Dillet V, Van Etten RL, Bashford D. J. Phys. Chem. B. 2000; 104:11321.

196. Zhang M, Van Etten RL, Stauffacher CV. Biochemistry. 1994; 33:11097. [PubMed: 7537084]

197. Zhang M, Zhou M, Van Etten RL, Stauffacher CV. Biochemistry. 1997; 36:15. [PubMed: 8993313]

198. Hart JC, Burton NA, Hillier IH, Harrison MJ, Jewsbury P. Chem. Commun. 1997:1431.

199. Peters GH, Frimurer TM, Andersen JN, Olsen OH. Biophys. J. 1999; 77:505. [PubMed: 10388775]

200. Peters GH, Frimurer TM, Andersen JN, Olsen OH. Biophys. J. 2000; 78:2191. [PubMed: 10777720]

201. Kolmodin K, Hansson T, Danielsson J, Aqvist J. ACS Symp. Ser. 1999; 721:370.

202. Hansson T, Nordlund P, Aaqvist J. J. Mol. Biol. 1997; 265:118. [PubMed: 9020976]

203. Kolmodin K, Aqvist J. FEBS Lett. 1999; 456:301. [PubMed: 10456328]

204. Kolmodin K, Aqvist J. Int. J. Quantum Chem. 1999; 73:147.

205. Feierberg I, Aqvist J. Theor. Chem. Acc. 2002; 108:71.

206. Guallar V, Jacobson M, McDermott A, Friesner RA. J. Mol. Biol. 2004; 337:227. [PubMed: 15001364]

207. Lennartz C, Schaefer A, Terstegen F, Thiel W. J. Phys. Chem. B. 2002; 106:1758.

208. Amyes TL, O'Donoghue AC, Richard JP. J. Am. Chem. Soc. 2001; 123:11325. [PubMed: 11697989]

209. Dewar MJS, Dieter KM. Proc. Natl. Acad. Sci. U.S.A. 1985; 82:2225. [PubMed: 3857576]

210. Jencks, WP. Catalysis in Chemistry and Enzymology. New York: Dover Publication, Inc; p. 1987

211. Warshel A, Aaqvist J, Creighton S. Proc. Natl. Acad. Sci. U.S.A. 1989; 86:5820. [PubMed: 2762299]

212. Verschueren KH, Seljee F, Rozeboom HJ, Kalk KH, Dijkstra BW. Nature. 1993; 363:693. [PubMed: 8515812]

213. Stucki G, Thuer M. Environ. Sci. Technol. 1995; 29:2339. [PubMed: 22280276]

214. Verschueren KHG, Franken SM, Rozeboom HJ, Kalk KH, Dijkstra BW. J. Mol. Biol. 1993; 232:856. [PubMed: 8355275]

215. Prince RC. Trends Biochem. Sci. 1994; 19:3. [PubMed: 8140618]

216. Franken SM, Rozeboom HJ, Kalk KH, Dijkstra BW. EMBO J. 1991; 10:1297. [PubMed: 2026135]

217. Devi-Kesavan LS, Gao J. J. Am. Chem. Soc. 2003; 125:1532. [PubMed: 12568613]

218. Nam K, Gao J. 2006 Manuscript in preparation.

219. Soriano A, Silla E, Tunon I, Marti S, Moliner V, Bertran J. Theor. Chem. Acc. 2004; 112:327.

220. Shurki A, Strajbl M, Villa J, Warshel A. J. Am. Chem. Soc. 2002; 124:4097. [PubMed: 11942849]

221. Lightstone FC, Zheng Y, Maulitz AH, Bruice TC. Proc. Natl. Acad. Sci. U.S.A. 1997; 94:8417. [PubMed: 9237991]

222. Maulitz AH, Lightstone FC, Zheng Y, Bruice TC. Proc. Natl. Acad. Sci. U.S.A. 1997; 94:6591. [PubMed: 9192609]

223. Lightstone FC, Zheng Y, Bruice TC. J. Am. Chem. Soc. 1998; 120:5611.

224. Damborsky J, Kuty M, Nemec M, Koca J. J. Chem. Inf. Comput. Sci. 1997; 37:562.

225. Damborsky J, Bohac M, Prokop M, Kuty M, Koca J. Protein Eng. 1998; 11:901. [PubMed: 9862209]

226. Dombrosky J, Koca J. Protein Eng. 1999; 12:989. [PubMed: 10585505]

227. Hur S, Kahn K, Bruice TC. Proc. Natl. Acad. Sci. U.S.A. 2003; 100:2215. [PubMed: 12610210]

228. Lightstone FC, Zheng Y, Bruice TC. Bioorg. Chem. 1998; 26:169.

229. Lewandowicz A, Rudzinski J, Tronstad L, Widersten M, Ryberg P, Matsson O, Paneth P. J. Am. Chem. Soc. 2001; 123:4550. [PubMed: 11457241]

230. Davidson MM, Gould IR, Hillier IH. J. Chem. Soc., Perkin Trans. 1996; 2:525.

231. Hall RJ, Hindle SA, Burton NA, Hillier IH. J. Comput. Chem. 2000; 21:1433.

232. Guimaraes CRW, Repasky MP, Chandrasekhar J, Tirado-Rives J, Jorgensen WL. J. Am. Chem. Soc. 2003; 125:6892. [PubMed: 12783541]

233. Guo H, Cui Q, Lipscomb WN, Karplus M. Angew. Chem., Int. Ed. 2003; 42:1508.

234. Hur S, Bruice TC. J. Am. Chem. Soc. 2003; 125:1472. [PubMed: 12568595]

235. Strajbl M, Shurki A, Kato M, Warshel A. J. Am. Chem. Soc. 2003; 125:10228. [PubMed: 12926945]

236. Crespo A, Marti MA, Estrin DA, Roitberg AE. J. Am. Chem. Soc. 2005; 127:6940. [PubMed: 15884923]

237. Ranaghan KE, Ridder L, Szefczyk B, Sokalski WA, Hermann JC, Mulholland AJ. Org. Biomol. Chem. 2004; 2:968. [PubMed: 15034619]

238. Marti S, Andres J, Moliner V, Silla E, Tunon I, Bertran J. Chem.–Eur. J. 2003; 9:984. [PubMed: 12584715]

239. Lee YS, Worthington SE, Krauss M, Brooks BR. J. Phys. Chem. B. 2002; 106:12059.

240. Lyne PD, Mulholland AJ, Richards WG. J. Am. Chem. Soc. 1995; 117:11345.

241. Kienhoefer A, Kast P, Hilvert D. J. Am. Chem. Soc. 2003; 125:3206. [PubMed: 12630863]

242. Ranaghan KE, Mulholland AJ. Chem. Commun. 2004:1238.

243. Jencks WP. Adv. Enzymol. Relat. Areas Mol. Biol. 1975; 43:219. [PubMed: 892]

244. Lee JK, Houk KN. Science. 1997; 276:942. [PubMed: 9139656]

245. Shem DL, Gronert S, Wu W. Bioorg. Chem. 2004; 32:76. [PubMed: 14990306]

246. Feng WY, Austin TJ, Chew F, Gronert S, Wu W. Biochemistry. 2000; 39:1778. [PubMed: 10677227]

247. Hur S, Bruice TC. Proc. Natl. Acad. Sci. U.S.A. 2002; 99:9668. [PubMed: 12107279]

248. Lee T-S, Chong LT, Chodera JD, Kollman PA. J. Am. Chem. Soc. 2001; 123:12837. [PubMed: 11749542]

249. Miller BG, Butterfoss GL, Short SA, Wolfenden R. Biochemistry. 2001; 40:6227. [PubMed: 11371183]

250. van Bastelaere P, Vangrysperre W, Kersters-Hilderson H. Biochem. J. 1991; 278:285. [PubMed: 1831974]

251. Asboth B, Naray-Szabo G. Curr. Protein Pept. Sci. 2000; 1:237. [PubMed: 12369908]

252. Hu H, Liu H, Shi Y. Proteins. 1997; 27:545. [PubMed: 9141134]

253. Nicoll RM, Hindle SA, MacKenzie G, Hillier IH, Burton NA. Theor. Chem. Acc. 2001; 106:105.

254. Cameron CE, Benkovic SJ. Biochemistry. 1997; 36:15792. [PubMed: 9398309]

255. Miller GP, Benkovic SJ. Biochemistry. 1998; 37:6636. [PubMed: 9578547]

256. Osborne MJ, Schnell JR, Benkovic SJ, Dyson HJ, Wright PE. Biochemistry. 2001; 40:9846. [PubMed: 11502178]

257. Singh UC, Ramnarayan K, Hausheer FH. Free Energy Calc. Ration. Drug Des. 2001:253.

258. Cummins PL, Greatbanks SP, Rendell AP, Gready JE. J. Phys. Chem. B. 2002; 106:9934.

259. Maglia G, Allemann RK. J. Am. Chem. Soc. 2003; 125:13372. [PubMed: 14583029]

260. Ferrer S, Silla E, Tunon I, Marti S, Moliner V. J. Phys. Chem. B. 2003; 107:14036.

261. Hammes-Schiffer S. Curr. Opin. Struct. Biol. 2004; 14:192. [PubMed: 15093834]

262. Sikorski RS, Wang L, Markham KA, Rajagopalan PTR, Benkovic SJ, Kohen A. J. Am. Chem. Soc. 2004; 126:4778. [PubMed: 15080672]

263. Schnell JR, Dyson HJ, Wright PE. Annu. Rev. Biophys. Biomol. Struct. 2004; 33:119. [PubMed: 15139807]

264. Venkitakrisnan RP, Zaborowski E, Benkovic SJ, Dyson HJ, Wright PE. Biochemistry. 2004; 43:16046. [PubMed: 15609999]

265. Truhlar DG, Gao J, Garcia-Viloca M, Alhambra C, Corchado J, Sanchez ML, Poulsen TD. Int. J. Quantum Chem. 2004; 100:1136.

266. Pu J, Ma S, Gao J, Truhlar DG. J. Phys. Chem. B. 2005; 109:8551. [PubMed: 16852008]

267. Pu J, Ma S, Garcia-Viloca M, Gao J, Truhlar DG, Kohen A. J. Am. Chem. Soc. 2005; 127:14879. [PubMed: 16231943]

268. Thorpe IF, Brooks CL III. J. Phys. Chem. B. 2003; 107:14042.

269. Thorpe IF, Brooks CL III. Proteins: Struct., Funct., Bioinf. 2004; 57:444.

270. Thorpe IF, Brooks CL III. J. Am. Chem. Soc. 2005; 127:12997. [PubMed: 16159295]

271. Radkiewicz JL, Brooks CL III. J. Am. Chem. Soc. 2000; 122:225.

272. Rod TH, Radkiewicz JL, Brooks CL III. Proc. Natl. Acad. Sci. U.S.A. 2003; 100:6980. [PubMed: 12756296]

273. Falzone CJ, Wright PE, Benkovic SJ. Biochemistry. 1994; 33:439. [PubMed: 8286374]

274. Li L, Wright PE, Benkovic SJ, Falzone CJ. Biochemistry. 1992; 31:7826. [PubMed: 1510968]

275. Wong KF, Watney JB, Hammes-Schiffer S. J. Phys. Chem. B. 2004; 108:12231.

276. Greatbanks SP, Gready JE, Limaye AC, Rendell AP. Proteins: Struct., Funct., Genet. 1999; 37:157. [PubMed: 10584062]

277. Cha Y, Murray CJ, Klinman JP. Science. 1989; 243:1325. [PubMed: 2646716] Schowen RL, Huskey WP. J. Am. Chem. Soc. 1983; 105:5704.

278. Rucker J, Cha Y, Jonsson T, Grant KL, Klinman JP. Biochemistry. 1992; 31:11489. [PubMed: 1445883]

279. Glickman MH, Wiseman JS, Klinman JP. J. Am. Chem. Soc. 1994; 116:793.

280. Kohen A, Jonsson T, Klinman JP. Biochemistry. 1997; 36:6854.

281. Alhambra C, Sanchez ML, Corchado JC, Gao J, Truhlar DG. Chem. Phys. Lett. 2002; 355:388.

282. Abe I, Rohmer M, Prestwich GD. Chem. Rev. 1993; 93:2189.

283. Poralla K. BIO spektrum. 1998; 4:32.

284. Woodward RB, Bloch K. J. Am. Chem. Soc. 1953; 75:2023.

285. Corey EJ, Virgil SC, Sarshar S. J. Am. Chem. Soc. 1991; 113:8171.

286. Wendt KU, Schulz GE, Corey EJ, Liu DR. Angew. Chem., Int. Ed. 2000; 39:2812.

287. Major DT, Zhang Y, Truhlar DG, Gao J. 2006 Unpublished results.

288. Alhambra C, Corchado J, Sanchez ML, Garcia-Viloca M, Gao J, Truhlar DG. J. Phys. Chem. B. 2001; 105:11326.

289. Alhambra C, Byun K, Gao J. ACS Symp. Ser. 1998; 712:35.

290. Gao J, Friendorf M. J. Phys. Chem. A. 1997; 101:3182.

291. Eichinger M, Tavan P, Hutter J, Parrinello M. J. Chem. Phys. 1999; 110:10452.

292. Pu J, Gao J, Truhlar DG. Chem Phys Chem. 2005; 6:1853. [PubMed: 16086343]
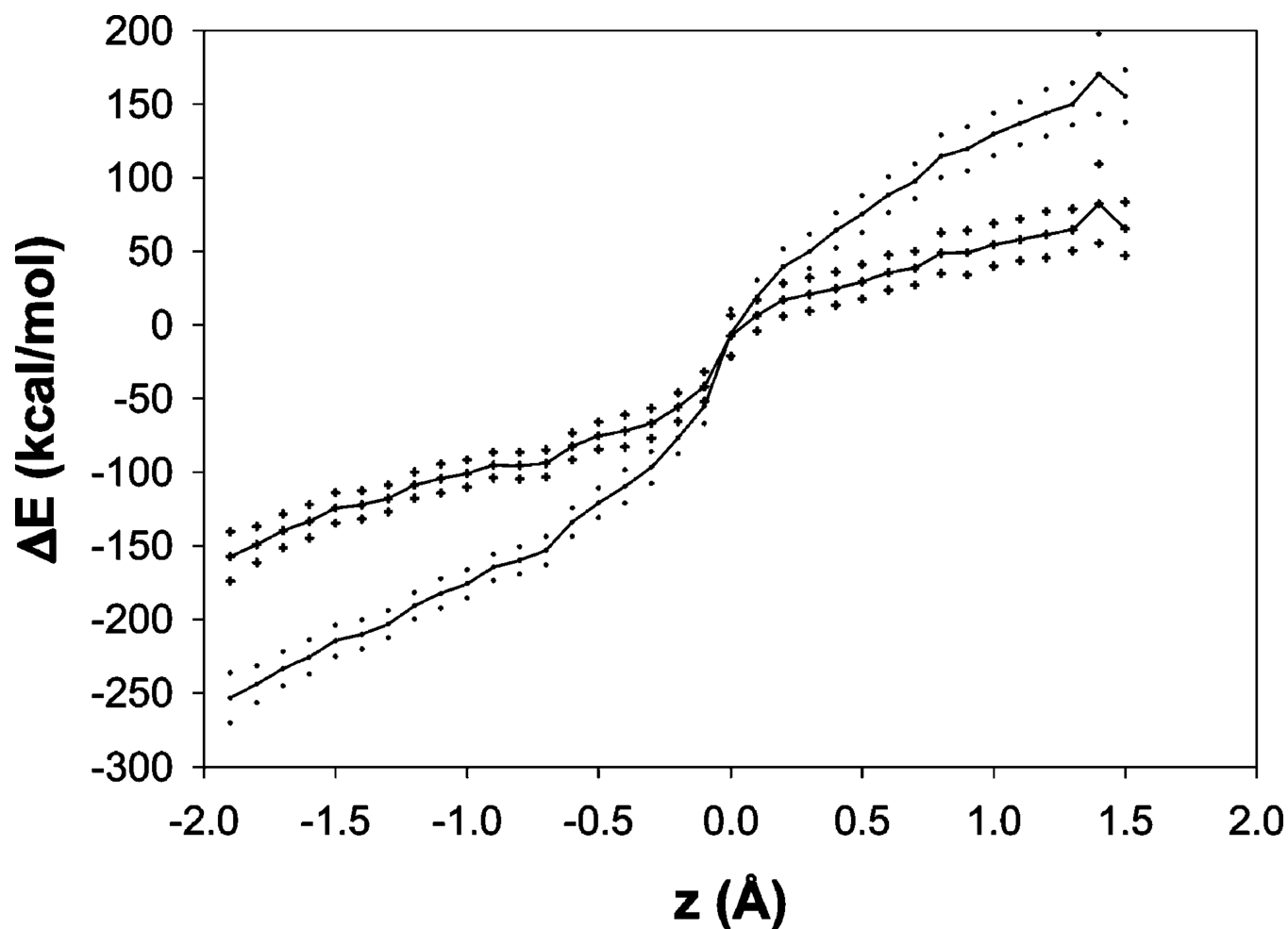
**Figure 1.**
Energy gap reaction coordinate calculated including the Morse potential for the C–H4 bond
(●) or without including it (+) as a function of the geometric reaction coordinate used to
study the hydride transfer reaction in DHFR. For both cases, the solid curve joins the
average values over bins of width 0.1 Å, and the symbols above or below are the result of
adding or subtracting the corresponding standard deviation.
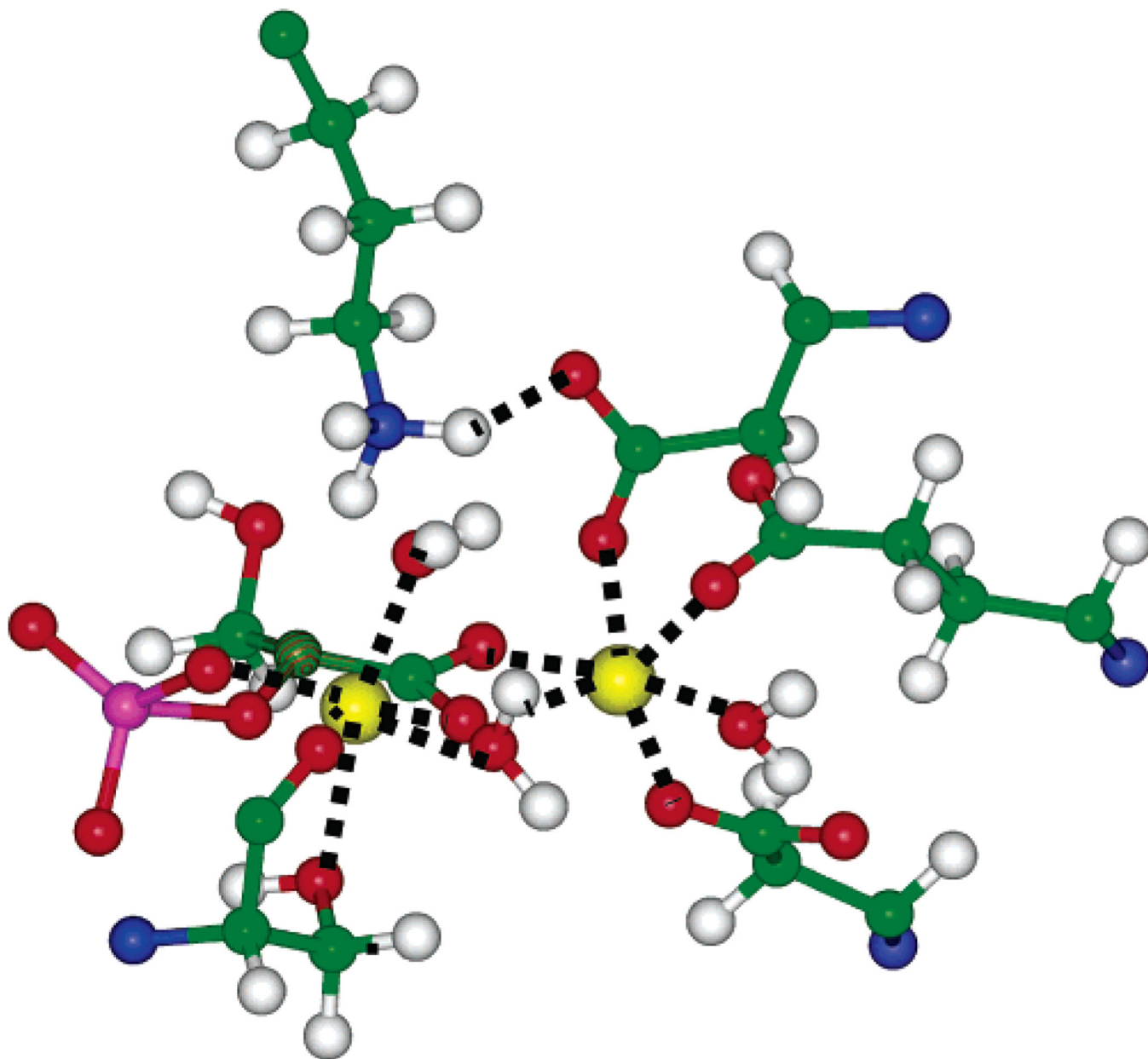
**Figure 2.**
The active site of enolase modeled in combined QM/MM simulations.
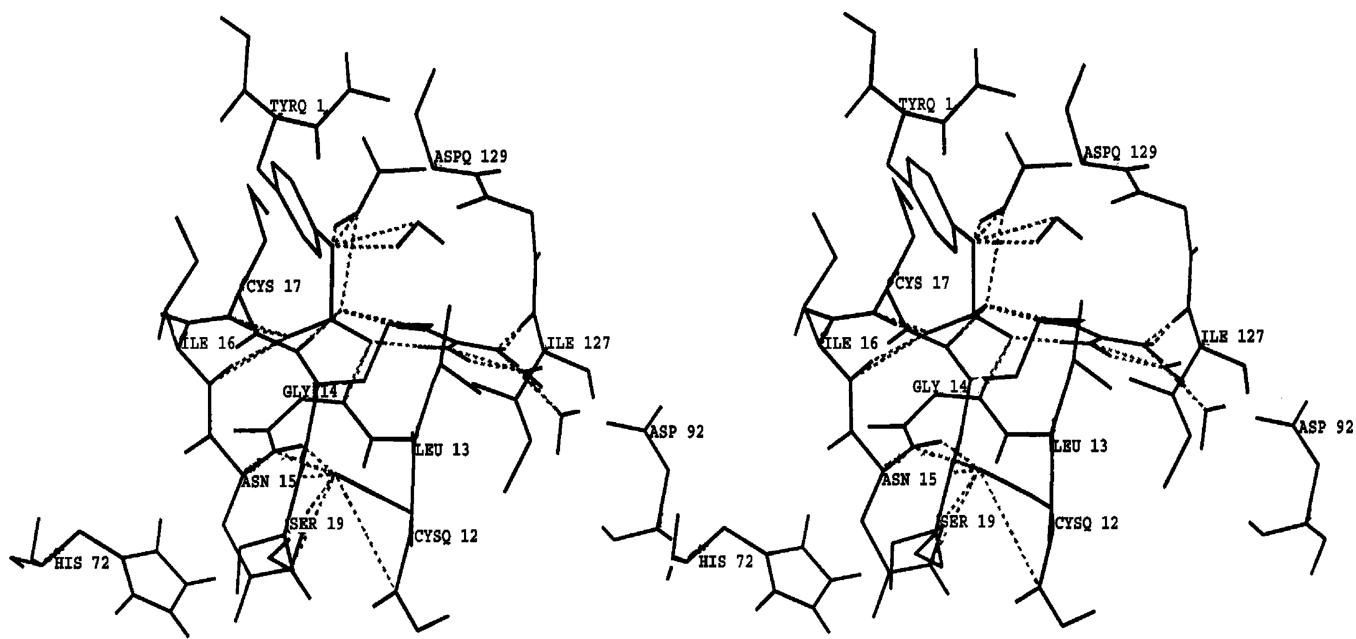
**Figure 3.**
Stereoview of the active site of low-molecular-weight protein tyrosine phosphatase that illustrates the activation of Cys12 nucleophile and phosphotyrosine binding.
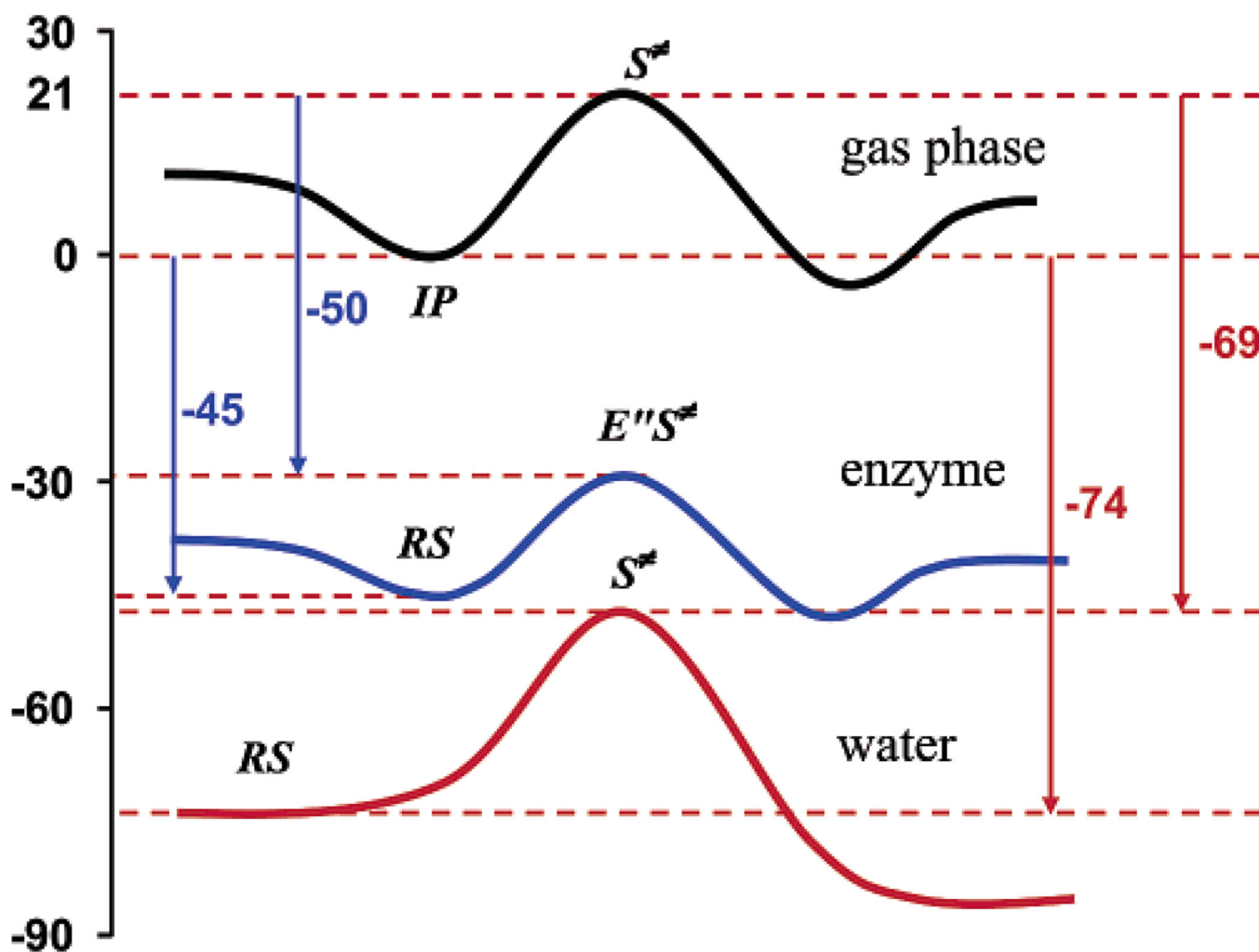
**Figure 4.**
Schematic energy diagram for the nucleophilic displacement of chloride by a carboxylate nucleophile in the gas phase (black), in aqueous solution (red), and in haloalkane dehalogenase (blue). The electrostatic components of solvation free energies have been computed by free energy perturbation theory using particle-mesh Ewald and combined QM/MM simulations; their values are indicated alongside the vertical arrows, corresponding to a standard state of 1 M concentration. IP is ion–dipole complex.
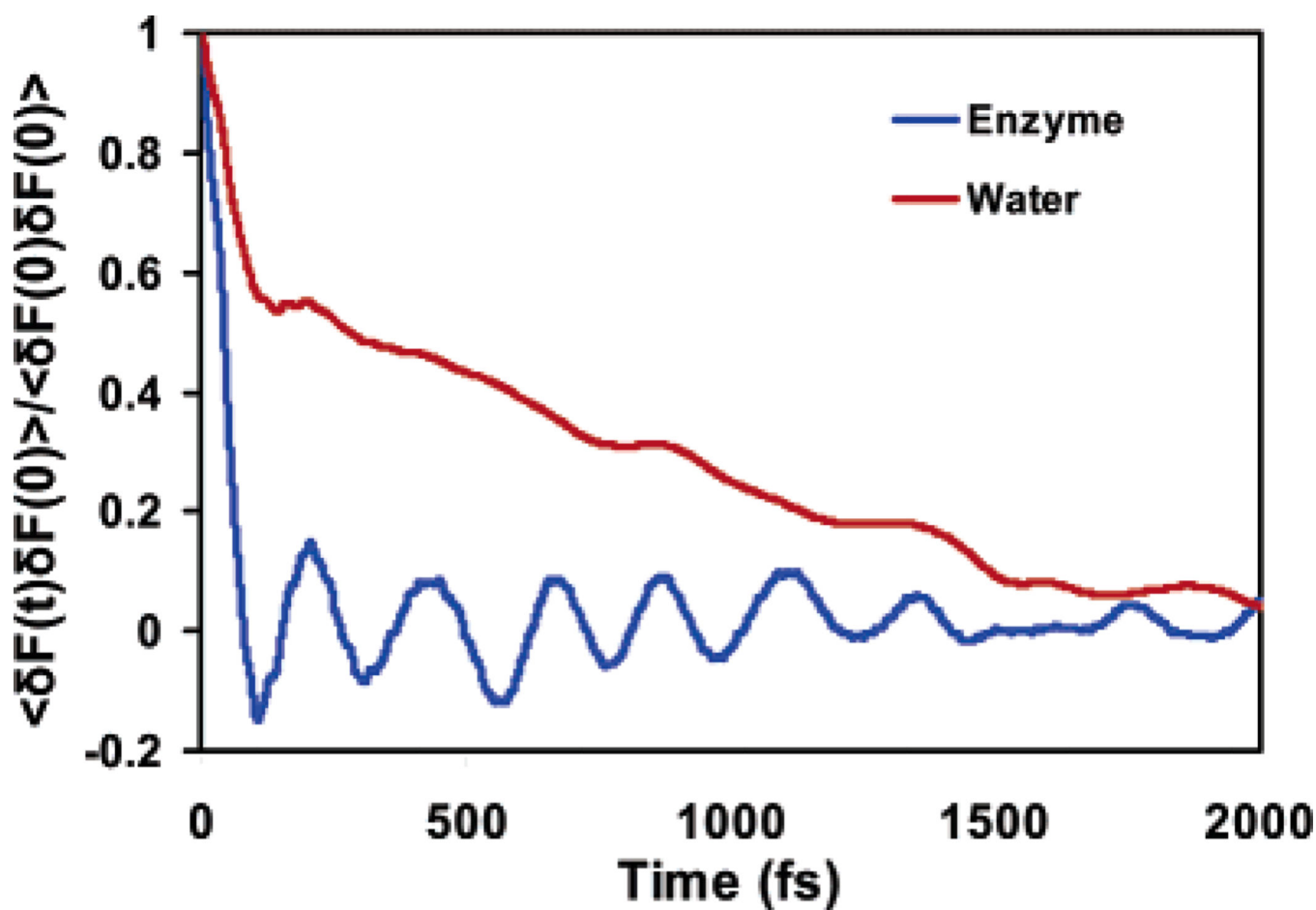
**Figure 5.**
Autocorrelation function $\langle \delta F(t) \delta F(0) \rangle$, where $\delta F(t)$ is the fluctuation of the gradient of the potential directed along the reaction coordinate at the transition state ($F_q(t) = -[\delta V/\delta q]_{q=q(\text{TS})}$) for the nucleophilic substitution reaction of dichloroethane by acetate ion in water (red) and by an aspartate residue in haloalkane dehalogenase (blue).

**PMF for the Orotate Decarboxylation Reaction**
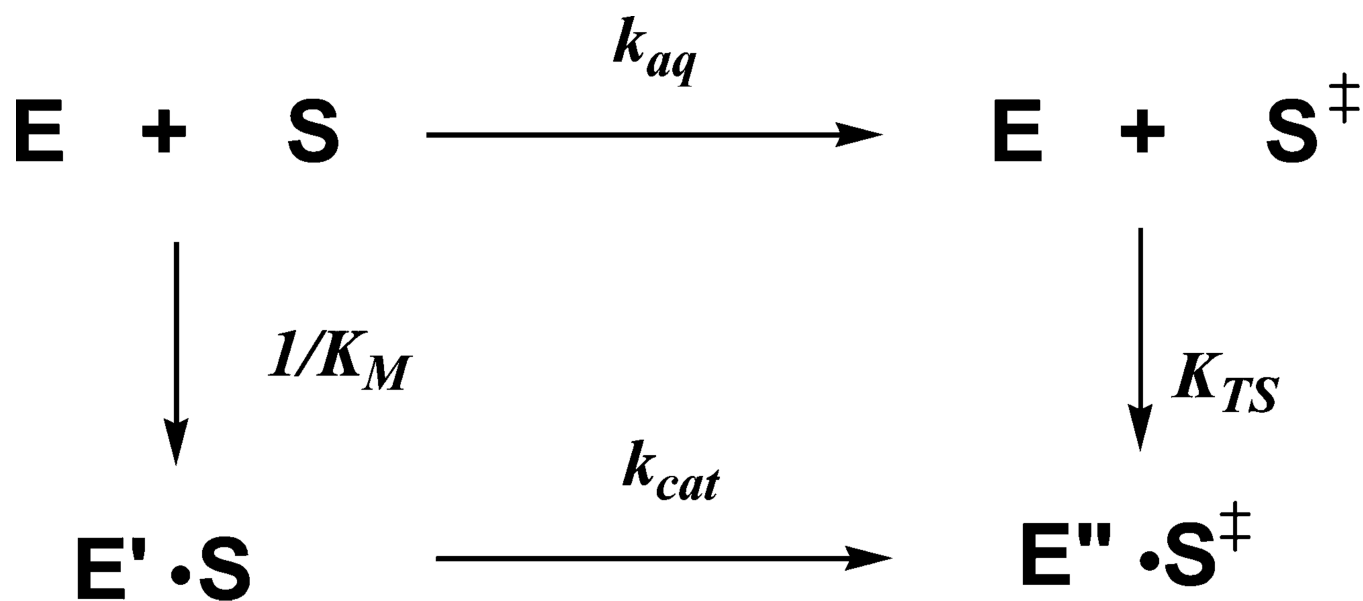


**PMF of ODCase D70A-Mutant Reaction**
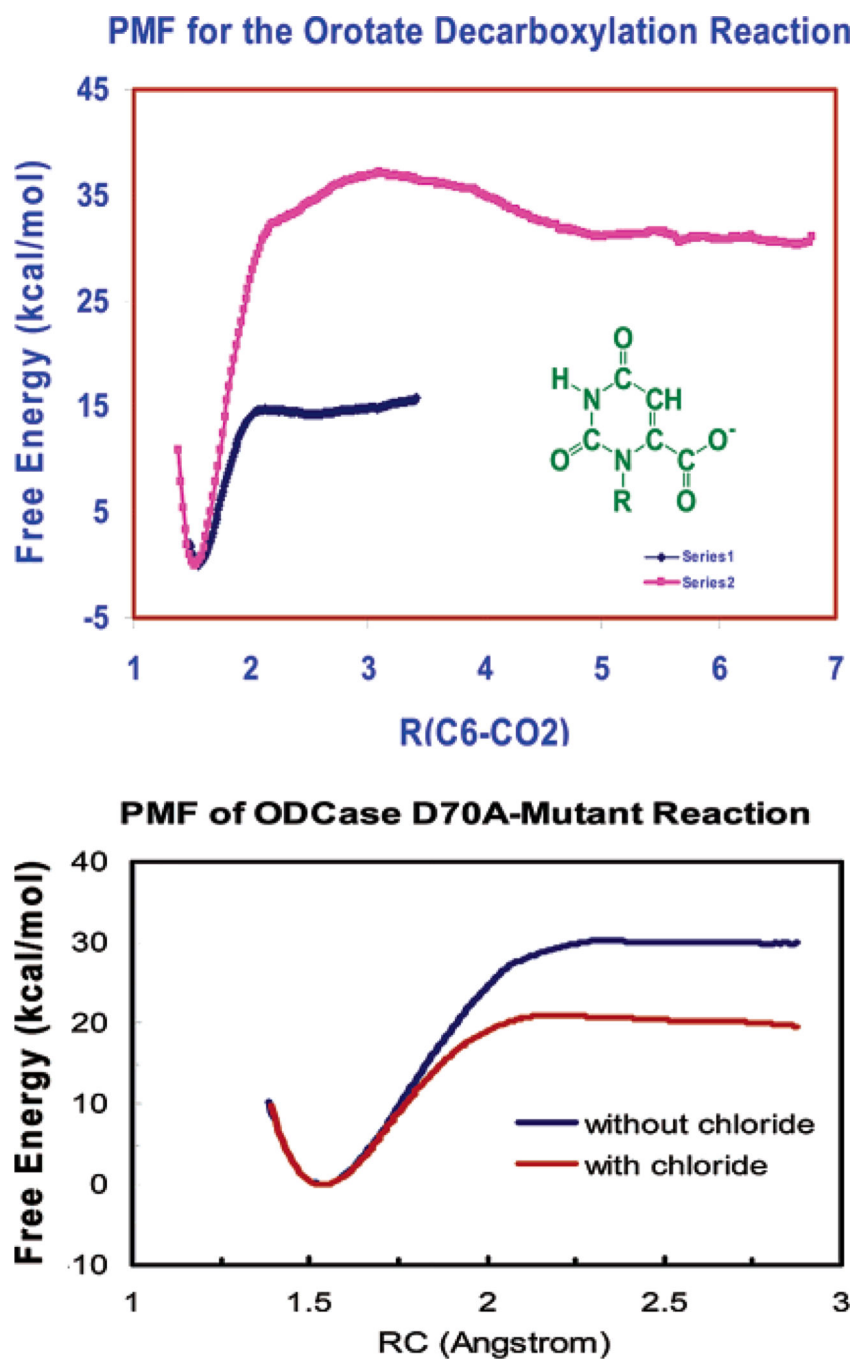
**Figure 6.**
Computed potentials of mean force for the decarboxylation reaction of OMP in water and in the wild-type enzyme ODCase (top) and for the reaction in the Asp70Ala mutant with and without a chloride ion in the active site (bottom).
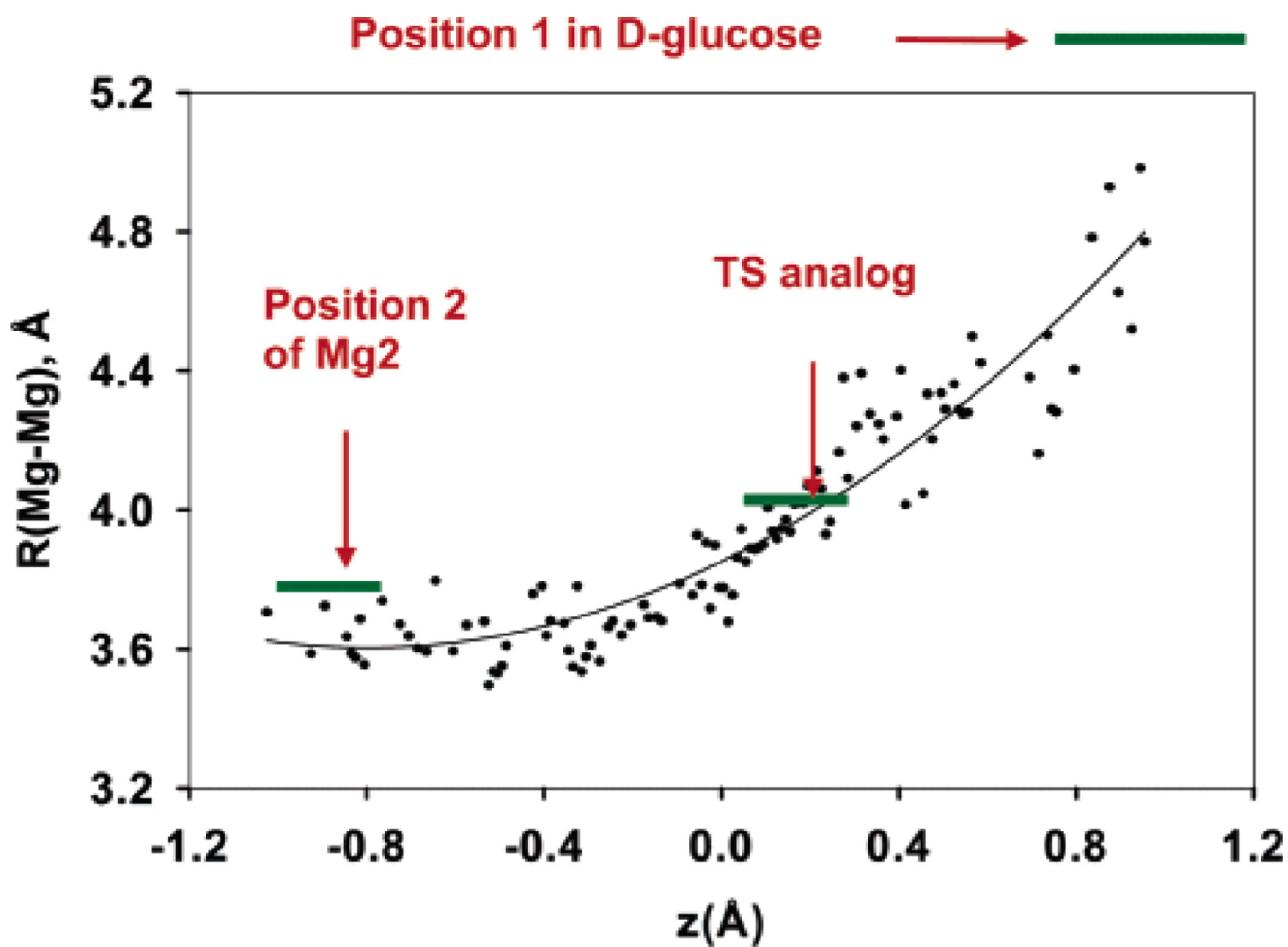
**Figure 7.**
Computed Mg–Mg distance as a function of the hydride transfer reaction coordinate for conversion of xylose to xylulose in xylose isomerase. The magnesium separation is accompanied by the migration of the hydride from the C2 carbon to the C1 position, resulting in a 1-alkoxide anion that favors strong binding with Mg2.
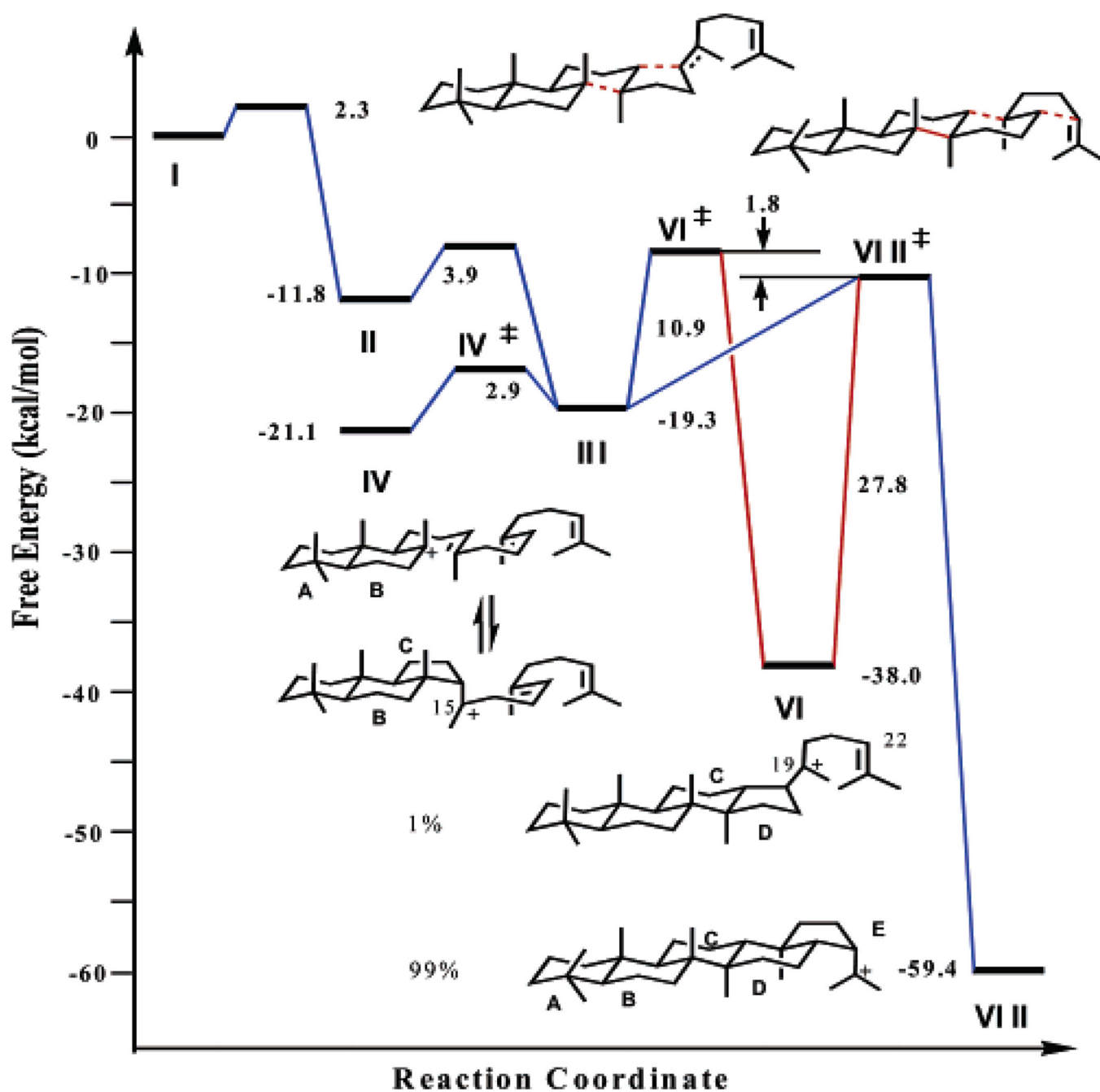
**Figure 8.**
Relative free energies for key reaction intermediates and transition states in the mechanism of squalene cyclization (Scheme 4) in squalene–hopene cyclase. The minimum connected by red lines is proposed as a thermodynamic trap, leading to the 1% observed side products.

$$E + S \xrightarrow{k_{aq}} E + S^{\ddagger}$$

$$\downarrow 1/K_M \qquad\qquad\qquad \downarrow K_{TS}$$

$$E' \cdot S \xrightarrow{k_{cat}} E'' \cdot S^{\ddagger}$$

**Scheme 1.**
Pseudothermodynamic Cycle That Relates the Equilibrium and Kinetic Parameters for the
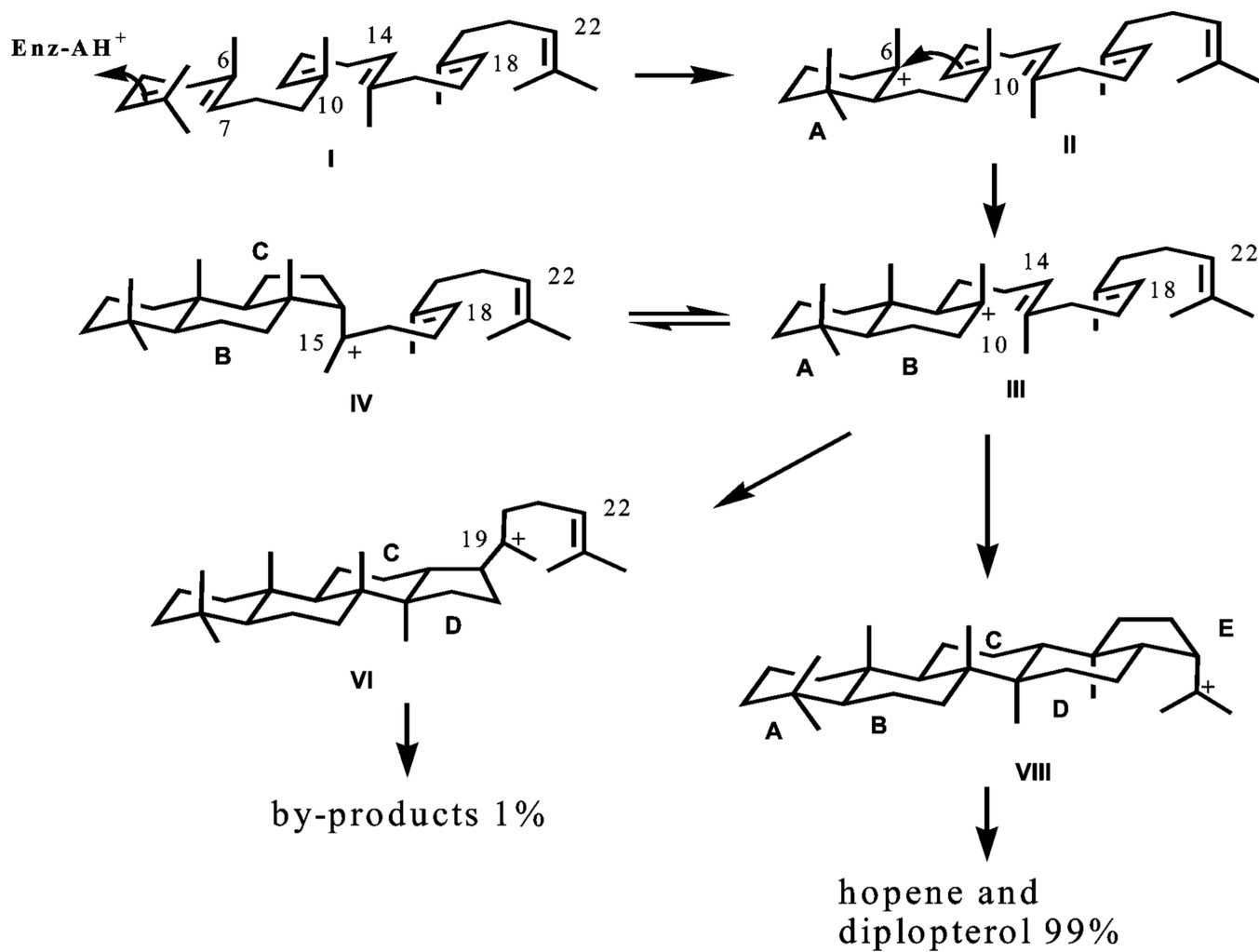Enzymic Reaction and the Uncatalyzed Reaction in Water
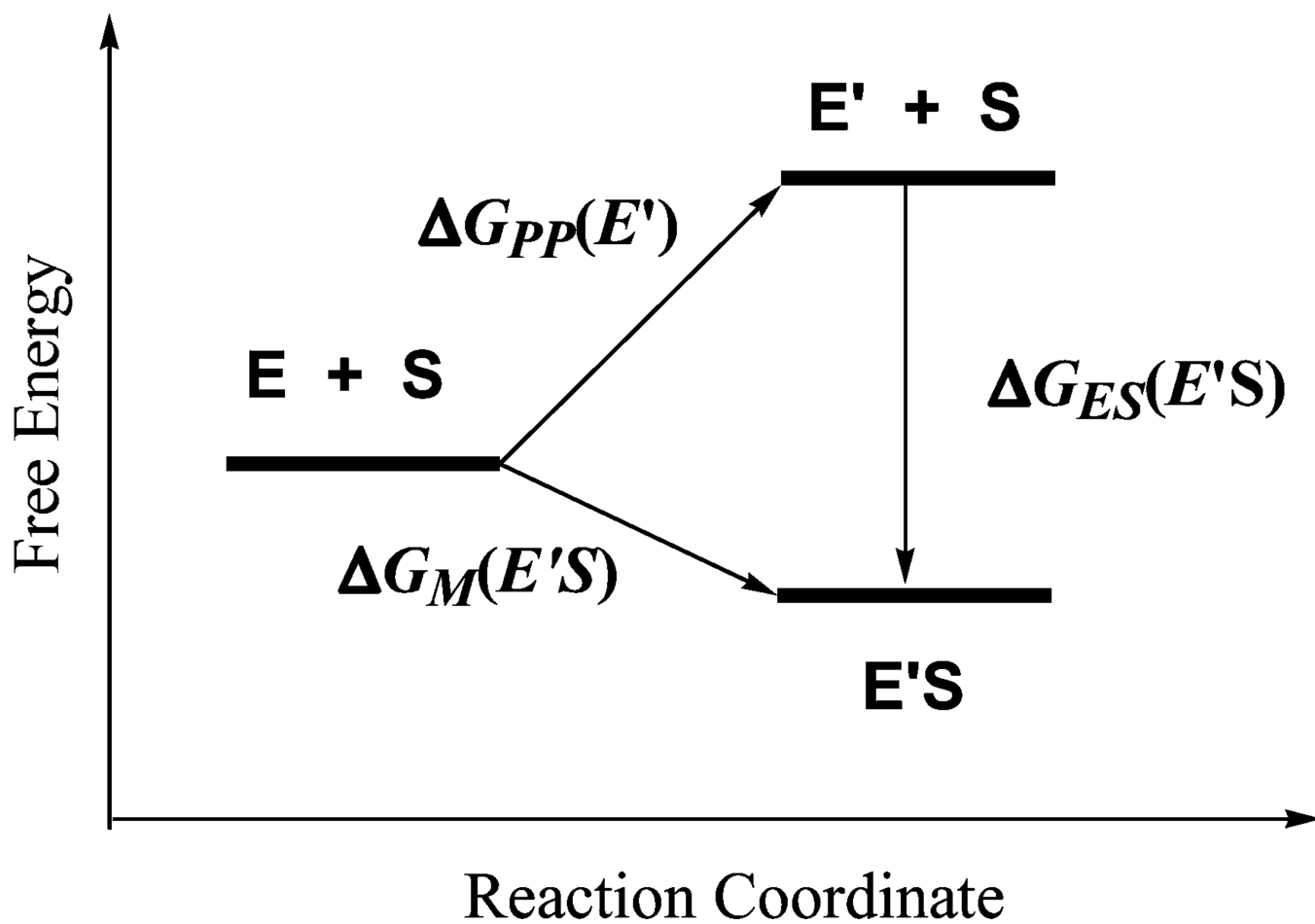
**Scheme 2.**
Schematic Representation of the Binding Free Energy Decomposition Analysis for Enzyme (E) and Substrate (S) Interactions
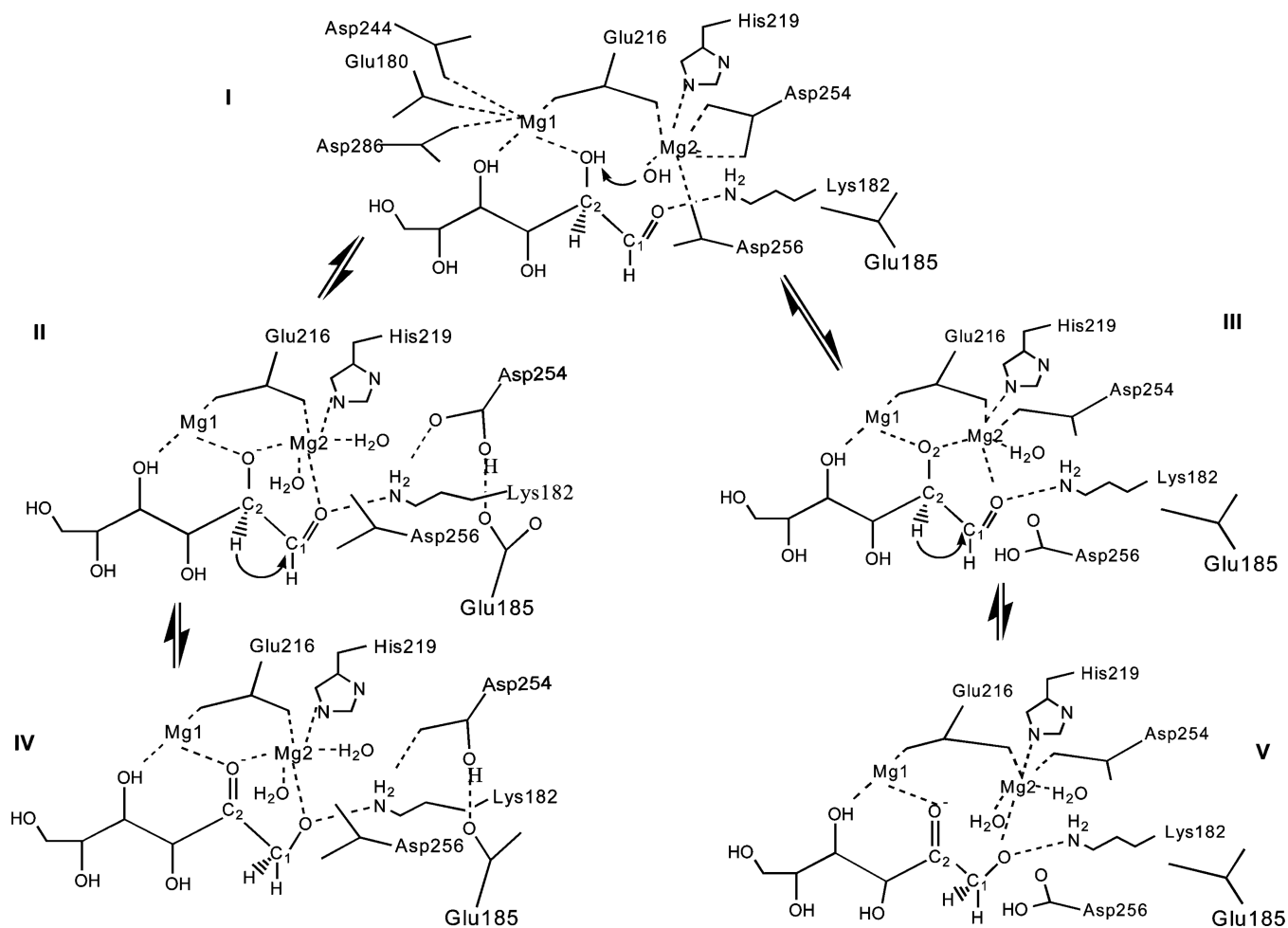
**Scheme 3.**
Schematic Representation of the Mechanisms Proposed by Petsko and Co-workers (I → II → IV) and Whitlow et al. (I → III → V) for the Proton and Hydride Transfer Steps

**Scheme 4.**
Proposed Carbocation Cyclization Mechanism in Squalene–Hopene Cyclase Based on the
Free Energy Diagram of Figure 8

**Table 1**

A List of the Enzymes and the Associated Chemical Transformations that Are Discussed in This Paper

| | |
|---|---|
| Acyl-CoA dehydrogenase (ACAD, MACD, BACD) |  |
| Chorismate mutase | Chorismate ⟶ Prephanate |
| Dihydrofolate reductase (DHFR) |  |
| Enolase |  |
| Haloalkane dehalogenase (DhlA) | $CH_2Cl—CH_2Cl$ ⟶ $CH_2Cl—CH_2OH$ |
| Methylamine dehydrogenase (MADH) | $CH_3NH_2$ ⟶ $CH_2=O$ + $NH_3$ |
| Orotidine 5'-monophosphate decarboxylase (ODC) |  |
| Protein tyrosine phosphatase (PTP) |  |
| Trichodiene cyclase (TDC) |  |
| Triosephosphate isomerase (TIM) |  |
| Squalene-Hopane cyclase (SHC) |  |
| Xylose isomerase (XyI) |  |

**Table 2**

Computed Kinetic Isotope Effects ($k_H/k_D$) Using Ensemble-Averaged Variational Transition State Theory with Multidimensional Tunneling for Hydrogen Transfer Reactions, as Compared to Experiment

| enzyme reactions | EA-VTST[a] | EA-VTST/MT[b] | expt | ref |
|---|---|---|---|---|
| Primary | | | | |
| enolase | 3.7 | 3.5 | 3 | 120 |
| liver alcohol dehydrogenase[c] | 6.7 | 7.5 | 7–8 | 288 |
| methylamine dehydrogenase | 5.9 | 18 | 17 | 281 |
| xylose isomerase | 1.8 | 3.8 | 3–4 | 150, 151 |
| dihydrofolate reductase | 2.5 | 2.8 | 3 | 122 |
| acyl-CoA dehydrogenase | 3.5 | 4.4 | 6.9–17 | 138 |
| Secondary | | | | |
| liver alcohol dehydrogenase[c] | 1.09 | 1.36 | 1.32 | 288 |
| dihydrofolate reductase | 1.03 | 1.13 | 1.13 | 122 |

[a]Includes quantization of vibrations but not tunneling.

[b]Also includes tunneling.

[c]$k_H/k_T$ (others are $k_H/k_D$).